# Estimation of Wax Deposition in Subsea Pipelines

A Thesis

Presented to

The Faculty of the Department of Mechanical Engineering

University of Houston

In Partial Fulfillment

Of the Requirements for the Degree

Master of Science

In Mechanical Engineering

By

Anthony Tatsis

August 2019

# Estimation of Wax Deposition in Subsea Pipelines

_____

Anthony Tatsis

Approved:

_____

Chair of the Committee
Dr. Matthew A. Franchek, Professor,
Mechanical Engineering

Committee Members:

_____

Dr. Karolos Grigoriadis, Professor,
Mechanical Engineering

_____

Dr. Cumaraswamy Vipulanandan, Professor,
Civil Engineering

_____

Dr. Suresh K. Khator, Associate Dean,
Cullen College of Engineering

_____

Dr. Pradeep Sharma, Professor,
Department Chair of Mechanical Engineering

**Acknowledgements**

My thanks and appreciation to my supervisor, Dr. Matthew Franchek for his technical guidance throughout the duration of this work and for his inspiring motivation that allowed me to reach further than I thought I would.

My thanks to the members of the committee Dr. Cumaraswamy Vipulanandan and Dr. Karolos Grigoriadis for the insight they provided through their constructive comments.

Warm thanks to Mr. Amine Meziou for his voluntary support that helped me to understand in depth the 2-phase flow model.

My sincere gratitude to Ms. Jenna Donnelly for all her efforts and support.

Finally, my special thanks to my wonderful wife, Thalia and my family who were always by my side and supported me in every step.

# Estimation of Wax Deposition in Subsea Pipelines

An Abstract
of a
Thesis
Presented to
The Faculty of the Department of Mechanical Engineering
University of Houston

In Partial Fulfillment
Of the Requirements for the Degree
Master of Science
In Mechanical Engineering

By
Anthony Tatsis

August 2019

**Abstract**

Developed is a multi-physics low dimensional model forecasting wax deposition rate within subsea production pipelines. This research employs experiments from 1-D and 2-D multiphase flow that have been successfully matched by a combined physics model on a closed-loop structure where the measuring length was 2.5m and the pipe inside diameter 0.0144m. The wax precipitation factor correlations used in 1-D and 2-D wax deposition models are valid only for 1-phase flows. Thus, to apply the 2-phase flow along these models the import of a coefficient is applied, directly related to the Gas Volume Fraction. Finally, there is a simulation that validates the model for 1-D, 1-phase closed loop system and a simulation for 1-D, 2-phase closed loop system. Then, the model is applied on a subsea pipeline for 1-D, 1-phase for a pipe of 0.305m ID, 80km long and for 2-D, 2-phase separately for a pipeline of same ID, 100m and 1000m long.

**Table of Contents**

**List of Figures**

**List of Tables**

**Nomenclature**

| | |
|---|---|
| $a$ | Solubility Function Coefficient a kg/m$^3$ K$^6$ |
| $b$ | Solubility Function Coefficient b °C |
| $c$ | Solubility Function Coefficient c °C |
| $C_P$ | Specific Heat Capacity at Constant Pressure J/(kg·K) |
| $C_{wb}$ | Wax Concentration in the Bulk Oil (kg/m$^3$) |
| $C_{ws}$ | Solubility of Wax in the Oil Solvent (kg/m$^3$) |
| $De$ | Effective Diffusivity of Wax Molecules into the Oil-Wax Gel (kg/m$^3$) |
| $D_{wo}$ | Molecular diffusivity (m$^2$/s) |
| $E_L$ | Liquid Holdup |
| $E_{LTrans}$ | Liquid Holdup for the Transition Flow |
| $E_{SL}$ | Non-Slip Liquid Holdup (m$^3$/m$^3$) |
| $f_n$ | No-slip Darcy Friction Factor |
| $f_{tp}$ | Two-phase Friction Factor |
| $Fr$ | Froude Number |
| $\bar{F}_w$ | Weight Fraction of Wax in the Deposit (kg/kg) |
| $h_i$ | Internal Concective Heat Transfer Coefficient W/(m$^2$K) |
| $h_o$ | External Concective Heat Transfer Coefficient W/(m$^2$K) |
| $k_1$ | Precipitation Coefficient by Singh et al. (m/s) |
| $k_M$ | Precipitation Coefficient by IHMT method (m/s) |
| $L_1$,$L_2$,$L_3$,$L_4$ | Beggs and Brill Correlation: Non-dimensional Numbers |
| $\dot{m}$ | Mass Flow Rate (kg/s) |
| $Nu$ | Nusselt number |
| $OD$ | Outside Diameter (m) |
| $Pr$ | Prandtl Number |
| $Q_G$ | Gas Flow Rate (m$^3$/s) |
| $Q_L$ | Liquid Flow Rate (m$^3$/s) |
| $Re$ | Reynolds number |
| $Re_n$ | No-slip Reynolds Number |
| $Re_{tp}$ | Two-Phase Reynolds Number |
| $s$ | Beggs and Brill correlation parameter |
| $Sc$ | Schmidt Number |
| $Sh$ | Sherwood Number |
| $T_i$ | Oil-Gel Interface Temperature (·C) |
| $U$ | Overall Heat Transfer Coefficient W/(m$^2$K) |
| $U_\infty$ | Undisturbed uniform crossflow velocity (m/s) |
| $V_A$ | Molar Volume of the Paraffin (cm$^3$/mol) |
| $V_{SL}$ | Superficial Liquid Velocity (m/s) |
| $V_m$ | Total Mean Velocity (m/s) |
| $\alpha$ | Average Aspect Ratio of the Wax Crystals in the Deposit |
| $\beta_{eq}$ | Equivalent Bulk Modulus (Pa) |
| $\gamma$ | Dimensionless Parameter for the Diffusivity Calculation |
| $\mu$ | dynamic viscosity (Pa s) |
| $\mu_{eq}$ | Equivalent Viscosity (Pa s) |
| $\mu_n$ | No-slip Viscosity (Pa s) |
| $\rho$ | Density (kg/m$^3$) |
| $\rho_{eq}$ | Equivalent density (kg/m$^3$) |
| $\rho_n$ | No-slip Density (kg/m$^3$) |

| | |
|---|---|
| $\rho^0_{eq}$ | Equivalent density at atmospheric pressure (kg/m$^3$) |
| $\rho_{gel}$ | Gel Density (kg/m$^3$) |

## Chapter 1: Introduction

Oil and its by-products are omnipresent in the modern world and are a definitive trait of our era. From transportation fuel to high-end materials, our world would be different without petroleum. If oil ever runs out it will be the end of the world as we know it, in ironic contrast to the verse of the song 'It's The End Of The World'. And so it is that the oil industry ever expands, searching for the precious material in the most remote and hostile environments of the earth. Be it the North Pole or the depths of the ocean it is found and extracted, at no low cost or without sophisticated equipment. The extraction of oil from the seabed has led to the emergence of an entirely new branch of technology, known as subsea engineering. The term is justified by the problems that must be overcome in production and by further challenges set by environmental regulations.

To begin with, the conditions at the bottom of the sea set certain constraints on the equipment. While descending to reach the seabed, the pressure of the water increases about 1atm every 10 meters and at a depth of 1 km or more the pressure amounts to the scale of hundreds of atmospheres. Furthermore, there are subsea streams the strain from which adds up on the pipes and cables descending to the depths The pipelines, the control systems, sensors and other equipment must be sturdy enough to routinely withstand such pressures and strains. Moreover, the daylight does not penetrate in depths below 1 km which imposes a requirement for strong light sources. All controls and operations have to be remote as well. Thus, a system parallel to the oil pipeline must be developed to transfer enough power to operate the production and the parallel systems. In addition, there is galvanic corrosion, exaggerated by the static electricity difference between surface and seabed. All equipment and specially the stable components are covered with protective layers of anti-corrosive material. Finally, the crude oil itself sometimes comes out of the earth at high pressure outbursts which can damage the pipelines from the inside leading to the installation of safety valves and hydraulic pressure safety systems.

The oil extraction equipment, the safety, sensing and controlling systems, the powerlines and the oil transportation lines are integrated into what is called the subsea architecture (Figure 1).

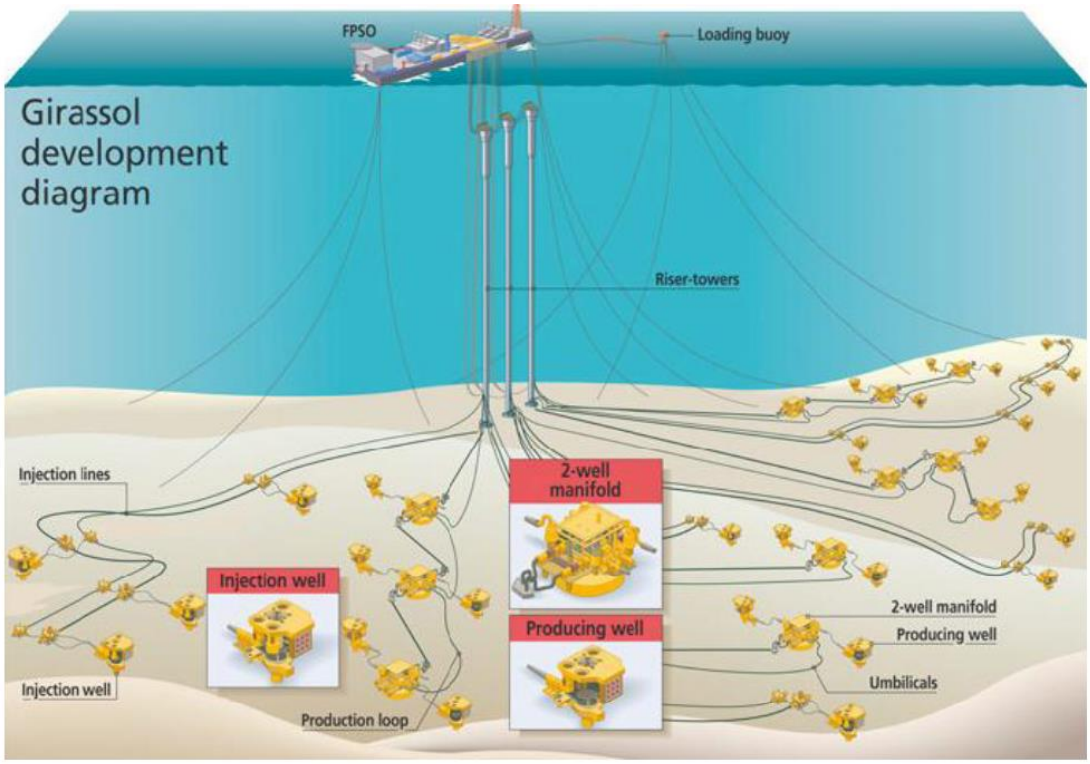


**Figure 1:** Subsea Architecture **(Terrell, 2014)**

Once the subsea architecture is installed and operation commences, there is still one major problem that must be dealt with and that is wax deposition. The crude oil that comes out of the earth is hot, its temperature ranging between 80 °C and 120 °C and rarely it reaches up 200 °C. As it travels along the pipeline its temperature drops resulting in the solidification of the heaviest of its components. Some of them form agglomerates which keep flowing till the exit but increase the oil's viscosity while others are diffused and attached to the wall. The latter are deposited along the pipeline gradually plugging it, which results in the reduction of the oil flow rate and even in complete halt of the flow.

**Figure 2:** Plugged Pipeline. **(Flatern, 1997)**

The richer the oil is in waxes or asphaltene, the faster the wax deposition rate. Wax deposition is remediated thermally by pouring hot oil in the pipe to melt away the wax deposit. Another way is by use of chemicals that dissolve or react with the wax deposit. In either case, the production must be held until the cleaning procedure is over. Cleaning the pipeline with scrapers and cutters is another, cheap solution, known as pigging for which oil production does not need to halt. However, if the pigging mechanism meets high resistance it may stick inside the pipeline causing major disruptions.

**Figure 3:** Pigging Mechanism **(LTD, 2012)**

In the upstream industry there is a fierce competition driven by the global need in oil. In this environment, forecasting of the production capabilities of a site is imperative for long term and short term management. Being able to calculate the operational expenses of a production facility for the next decades makes the difference in deciding upon investing on that facility. For near feature decisions, knowing the maximum production level for the next days might give the edge over competition. In both cases, the production cost and production variation depend upon one factor, the wax deposition rate. It is important to have a forecast of the wax deposition thickness.

Given the need of the industry the purpose of this study is to give an estimation of the wax deposition in depth of time. As of today, experiments have been conducted in controlled environment to estimate the wax formation and deposition. Results of these experiments are used in commercial software programs but there is no published study regarding the wax deposition on a pipeline. This thesis combines one of the existing models (P.Singh, 2014) for wax deposition with fluid flow and heat transfer models to simulate the wax deposition on a pipeline. Whilst the wax deposition appears in every facility for transporting or storing oil, this study is focused on systems where the outside temperature is steady, which is the case in subsea systems.

In general, the factors that affect the wax deposition rate are mainly the temperature, the flow rate and secondarily the pressure. The lower the initial temperature of the crude oil, the earlier the wax deposit starts building up. In all cases the hydraulic resistance of the pipeline increases causing the flow to slow down. However, the wax deposit works as insulator, inducing a lower wax diffusivity and thus decreasing its own thickness increment rate. The wax agglomerates that do not deposit increase the viscosity of the fluid, further reducing the flow rate. A technical question set here is which case impedes the flow the most, the deposition of wax or the agglomeration of the wax precipitates that increase the fluid's viscosity? Throughout this circle of events the wax deposit keeps increasing but with different rates. This is attempted to be described in this study combining a heat transfer, a multi-phase flow and a wax deposition model.

## 1.1. Outline

In this section an outline is given on the thesis. Starting with Chapter 2:, the most significant literature on wax precipitation and deposition models is presented. At the beginning of Chapter 3: the most widely accepted wax deposition models, namely the Singh et al model and its offspring the Independent Heat Mass Transfer model (IHMT) are presented. Subsequently, the chapter gives a detailed description of the physics participating in the wax deposition which are the diffusivity of wax molecules in oil solvent, the solubility of wax in oil, the heat transfer in pipelines, the 2-phase flow and finally the IHMT model which could also be described as a multi-physics wax deposition model. Following with Chapter 4: all the models above are combined to provide a 2-phase wax deposition rate estimation. An algorithm is set that can be used for both 1-phase and 2-phase flow and for both 1-D and 2-D wax deposition models. In Chapter 5: the 1-D wax deposition is validated, then the 2-phase flow is added on the validated model and finally the algorithm is applied on a pipeline for 1-D and 2-D. Chapter 7 has a section for the conclusions which define a set of data with which this model is applicable and finally a section proposing future work on precipitation and diffusion correlations for 2-D, 2-phase models.

## Chapter 2: Literature Review

The accumulation of paraffin wax at the walls of wellbores, pipelines and reservoirs has been a subject of study for many decades. The first studies produced thermodynamic models for the formation of wax precipitates, which allowed the definition of conditions under which wax may deposit. Some of them namely are the Pedersen model (K.S.Pedersen, 1991), Coutinho's model (Coutinho, 1998) which is embedded in the UNIQUAC model available in software and finally the Lira-Galeana model (Lira-Galena, 1996). These were followed by models based on experimental data which combined heat transfer and flow models to give an estimation of wax deposition under certain conditions. Some of them namely are the RRR model (P. Rygg, 1998), the Matzain (Matzain, 2001), the Singh et al. model (P.Singh, 2000) used in this study, all of which are outlined in the following paragraphs. The Singh et al. model is attested by the scientific community and has been used in latter studies and commercial software.

At this point there are two main methods of forecasting the wax deposition. One method is combining thermodynamic models for wax precipitation and system identification techniques to build neural networks (A.Kamari, 2015) that learn to predict the wax deposition given enough data. The main disadvantage of this method is that it can only be applied once the facility already operates. Thus, these methods are outside the scope of this study whose focus in forecasting before building the whole subsea architecture. The second method is using multi-physics simulation to estimate the wax deposition rate combining a heat transfer model, a flow model and a wax deposition model usually the Singh et al. This method is used in this study and its formulation has been established by Huang, Lee, Fogler, Senra, Venkatesan (Z.Huang, 2011) and Singh et al (P.Singh, 2000), whose work is outlined below.

### 2.1.1. Wax Deposition Models

All wax deposition models outlined below follow the same formula pattern to estimate the thickness of the wax deposit. What changes in each model is the calculation of the parameters which depends on experimental data. The terminology used in many articles for the wax deposition is aging of the incipient wax-oil gel. That is because the interface between bulk oil and solid wax deposit is a semi-solid layer through which the wax molecules or particles are diffused.

### 2.1.2. The Rygg-Rydahl-Ronningsen Model

Rygg, Rydahl and Ronningsen wax model (P. Rygg, 1998), also known as the RRR model is a combination of functions each describing a different phenomenon. These are the pressure drop and regime changes, the viscous flow of the oil, the energy inputs and outputs, the wax behavior with change of pressure and temperature and finally the wax transport mechanism. The model is described by the formula:

$$l_{wax} = \frac{Vol_{wax}^{diff} + Vol_{wax}^{shear}}{(1-\phi)2\pi rL}, \quad (1)$$

where, $l_{wax}$ is the volume rate of deposited wax, r the internal pipe diameter, L is the pipe segment's length, $\phi$ is the wax porosity with values ranging from 0.6 to 0.9, $Vol_{wax}^{diff}$ the volume rate of wax deposited by diffusion and $Vol_{wax}^{shear}$ is the volume rate of wax deposited by shear dispersion. For each component of the oil mixture the deposition rate by diffusion is different (Calsep). These add up along the pipe wall surface and their total is given by

$$Vol_{wax}^{diff} = \sum_{i=1}^{N_w} \frac{D_i(\Delta C_i)S_f M_i}{\delta \rho_w} 2\pi rL, \quad (2)$$

where $N_w$ is the number of wax component, $D_i$ is the diffusion coefficient ($m^2/s$), $\Delta C_i$ is the concentration difference between the bulk phase and the wax phase for component $i$ , $S_f$ is the fraction of wetted perimeter by wax, $M_i$ is the molecular weight (g/mol), $L$ is the length of the pipe (m), $r$ is the effective inner pipeline radius to account for wax deposition (m), $\rho_w$ is the destiny of wax component $i$ ($kg/m^3$) and $\delta$ is the thickness of the laminar sub layer (m).

Bendiksen et al. (1991) provide the thickness of the laminar sub layer in the pipeline (Calsep):

$$\delta = \alpha\ 11.6\ \sqrt{2}\frac{D}{Re}\frac{1}{\sqrt{f}}, \tag{3}$$

where $D$ is the pipe diameter (m), Re is the Reynolds number and $f$ is the friction factor. $a$ is the allowed correction factor for tuning the wax layer thickness and is derived from experimental data. Finally, the deposition rate of wax by shear dispersion is given by the modified Burger et al. (1981) equation (Rosvold, 2008)

$$Vol_{wax}^{shear} = \frac{k\gamma A\phi_w}{\rho_w}. \tag{4}$$

The shear dispersion term contributes much less than the molecular diffusion term in the total wax deposition rate. Despite ignoring the shear stripping phenomenon and not accounting for the flow regime changes, the RRR model gives consistent and accurate results when compared with observed pressure losses for single and multiphase pipe systems (Calsep).

### 2.1.3. The Matzain Model

The Matzain model is a broader approach of the wax deposition as it includes the molecular diffusion, the shear dispersion and the shear stripping. The model is based on the diffusion coefficient, as per Wilke and Chang (C. R. Wilke, 1955), which was proposed by Burger et al. (1981) to be applied on the wax diffusion in oil pipelines. The diffusion is

$$D_w = 7.4\ 10^{-9} \frac{T_a(\xi M)^{0.5}}{\mu V^{0.6}}, \tag{5}$$

where $T_a$ is the absolute temperature (K) , $M$ is the molecular weight of the oil solvent (g/mol), $V$ is the wax molar volume (cc./g.mole), $\mu$ is the dynamic viscosity (μP) and $\xi$ is an association parameter representing the effective molecular weight of the solvent with respect to molecular diffusion. The wax molar volume $V$ is proportional to the absolute temperature. The formula of the Matzain model is given by (S.Cem, 2004)

$$\frac{d\delta}{dt} = \frac{\Pi_1}{1+\Pi_2} D_w \left[\frac{dC_w}{dT}\frac{dT}{dr}\right], \tag{6}$$

where $D_w$ is the Wilke-Chang diffusion coefficient, $C_w$ the concentratin of wax in solution (weight %), $r$ the pipe distance (m) and $T$ the bulk fluid temperature (°C). The coefficient $\Pi_1$ is related to the porosity effect on the wax deposition ratio and $\Pi_2$ is related to the shear stripping. Regarding $\Pi_1$, it is given by the formula (Calsep) (S.Cem, 2004)

$$\Pi_1 = \frac{C_1}{1-C_L/100}, \tag{7}$$

where, $C_L$ is the porosity effect coefficient and defines the amount of oil trapped in the wax layer, the Matzain constant is $C_1 = 15$ and

$$C_L = 100\left(1 - \frac{N_{Re,f}^{0.15}}{8}\right). \tag{8}$$

In equation (8), the dimensionless parameter $N_{Re,f}$ is a function of the effective inside diameter of the pipeline

$$N_{Re,f} = \frac{\rho_L v_L d_w}{\mu_L}, \tag{9}$$

For the Matzain constants $C_2 = 0.055$ and $C_3 = 1.4$, the $\Pi_2$ is given by the formula:

$$\Pi_1 = 1 + C_2 N_{SR}^{C_3}. \tag{10}$$

The values of the Matzain constants $C_2$ and $C_3$ are valid for single and two-phase flow. An explicit calculation of $N_{SR}$ for each flow regime is increasing the accuracy of the Matzain model and is given below:

Single phase and stratified wavy flows $$N_{SR} = \frac{\rho_L v_L \delta}{\mu_L}$$

Bubble and Slug flow $$N_{SR} = \frac{\rho_m v_L \delta}{\mu_L}$$

Annular flow $$N_{SR} = \frac{\sqrt{\rho_m \rho_L} v_L \delta}{\mu_L}.$$ (11)

The thermal gradient of the laminar sub layer can be obtained by (Rosvold, 2008):

$$\frac{dT}{dr} = \frac{(T_b - T_{wall})}{k_L} h_{wall}, \tag{12}$$

where $k_L$ is the thermal conductivity of the oil (W/mK), $h_{wall}$ is the inner wall heat transfer coefficient (W/m$^2$K), $T_b$is the bulk fluid temperature (K) and $T_{wall}$ is the inner wall surface temperature (K).

### 2.1.4. The Singh et al. Wax Deposition Model

This model is based on the thin-film concept which is supported by the deposition experiments of particles in wax layer, conducted by the University of Michigan. The element that Singh et al (2000) introduced with this model is the aging of the waxy gel layer. They also consider a mechanism of counter-diffusion (P.Singh, 2001).

The models prior to that proposed by Singh et al. assumed that there is thermodynamic equilibrium in the mass transfer boundary layer and so that the wax deposition rate is linearly proportional to the solubility $C_{ws}$ in the oil-wax deposit interface. This assumption has been proved wrong (Creek, 1999) and Singh et al. proposed a more valid formula:

General equation, followed by eq. (6) in the Matzain Model

$$\frac{dm_{deposit}}{dt} = -(2\pi r_i L) D_{wo} \frac{dC_{ws}}{dT} \frac{dT}{dr}\Big|_i . \tag{13}$$

Singh et al. introduced a term in the above equation that accounts for the difference between the wax concentration and the solubility. As the wax molecules are diffused near the wall, due to low temperatures, some of them precipitate. No longer being soluble in the bulk oil they do not diffuse into the deposit.

The Singh et al equation is

$$\bar{F}_w(t)\rho_{gel}\frac{dy}{dt} = \frac{k_1}{R}[C_{wb} - C_{ws}(T_i)] + \frac{D_e}{R}\frac{dC_{ws}}{dT}\frac{dT}{dr}\Big|_i , \tag{14}$$

where $k_1$ is the mass transfer coefficient and $\bar{F}_w$ the mass fraction of the wax in the in the deposit.

Another important element characterizing the radial mass flux and formation of the wax deposit, which was firstly introduced by Singh et al, is that of the wax deposit aging. As time goes by, more oil molecules are diffused out of the deposit and more wax molecules into it. This, has an effect on the insulation provided by the wax layer and an effect on the diffusion rate as the deposit is gradually saturated.

The governing equations for the wax deposition mechanism derived by Singh et al. were validated for laminar and turbulent flows of Re less than 5200 and have been embedded to various commercial simulators (P.Singh, 2014). The overall acceptance of these governing equations is the reason why this model was chosen for this Thesis.

However, the model proposed by Singh et al. overestimates the wax deposition rate and the higher the Re number the bigger the inaccuracy. The reason lies on the mass transfer coefficient $k_1$ which is calculated for laminar flows using the transport correlation of Seider and Tate (Seider, 1936) and Hausen (Hausen, 1943) for laminar flows

$$\begin{cases} Nu = 1.24\left(\frac{d}{L}RePr\right)^{(1/3)} \\ Sh = 1.24\left(\frac{d}{L}ReSc\right)^{(1/3)} \end{cases}. \quad (15)$$

There the axial, convective mass transfer to the radial, diffusive mass transfer ratio (expressed by the Sherwood number *Sh*) differs to the same ratio for turbulent flows. As a result, the Singh et al calculation for $k_1$ underestimates the precipitation rate in the boundary layer and the wax deposition rate is overestimated. The model is further described in the relevant section.

A method has been proposed by Venkatesan and Fogler (R.Venkatesan, 2004) to identify the lower bound of wax precipitation, namely the 'solubility method'. The correlation between the *Nu* and *Sh* numbers is

$$\begin{cases} Nu = 1.24\left(\frac{d}{L}RePr\right)^{(1/3)} \\ Sh = Nu\left.\frac{dC}{dT}\right|_i \frac{\Delta C}{\Delta T} \end{cases} . \tag{16}$$

In this model, all the wax molecules that do not solute are assumed to precipitate, thus never depositing. However, depending on the precipitation kinetics, the wax that does not solute earlier in the pipeline may solute later under conditions where the oil bulk is no longer supersaturated. The assumption above leads to a theoretical lowest extremum for the wax deposition rate (Z.Huang, 2011).

## 2.2. Combined Heat-Mass Transfer Analysis for Boundary Layers

Recent studies (Lee, 2008) (Z.Huang, 2011) have dealt with the mass transfer coefficient by implementing numerical methods to find the concentration and temperature near the oil-wax deposit interface. The model used in these studies calculates the Sherwood number with better accuracy and then the mass transfer coefficient $k_1$ which is now expressed as $k_M$. That model, which is integrated in the Singh et al mass balance and wax deposit aging equations, is implemented in this study. The model's equations are presented in sections 3.9, 3.11.1, 3.11.2, 0, 3.11.4, 3.11.4 and 3.11.5.

# Chapter 3: Wax Deposition and Solidification Models

Wax deposition is a natural process that depends on many factors, thus multi-physics models are required to make a wax deposition model. Flow, heat and mass transfer are developed in this chapter along with the wax deposition model. To concisely describe the overall process, this chapter's title refers to the end result of these phenomena combined together.

## 3.1. Wax Precipitation

Crude oil components include paraffins, naphthenes, aromatics, resins and asphaltenes. Paraffin molecules are the longest carbon-chains of these and the basis for paraffin wax. Wax exists in solution in crude oil but when temperature and pressure drop, it crystallizes around asphaltenes, formation fines, clay and corrosion products. This phenomenon is known as wax precipitation, the conditions under which it appears is known as cloud point and the temperature is referred to as the Wax Appearance Temperature (WAT). In every crude oil mixture there is a range of carbon chain molecules, each with different carbon number. Molecules with carbon number greater than the critical carbon number precipitate out of the oil body and form stable crystals. Crude oil mixtures from different wells may have a different critical carbon number and the conditions (temperature, pressure) at which wax crystals appear may be different. All the mixtures though follow the same pattern in phase transformation which depends mainly on the temperature and in second degree on pressure.

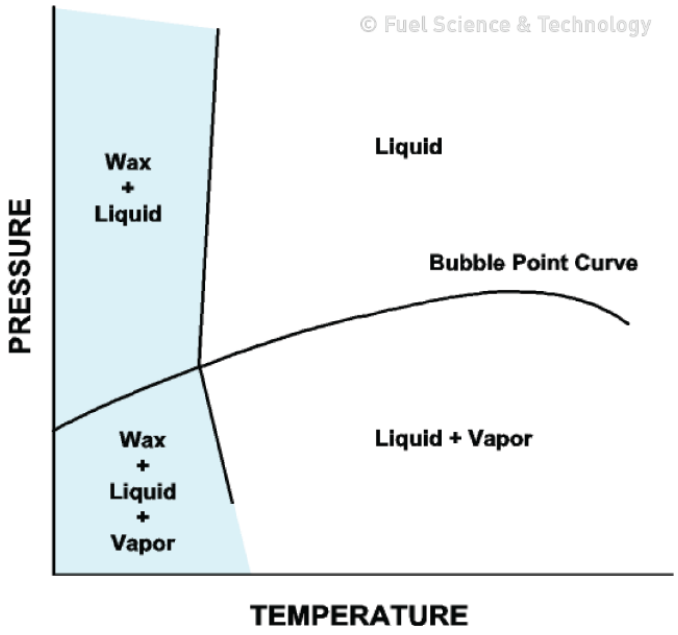


**Figure 4:** Pressure-Temperature Wax Precipitation **(Leontaritis, 1996)**

### 3.2. Wax Deposition Mechanism Proposed by Singh et al (P.Singh, 2000).

Wax deposits are formed by heavy hydrocarbon molecules that precipitate when they reach the relatively cold wall of the pipeline or reservoir. On a pipeline, these molecules are transferred radially by diffusion caused by the temperature difference between the warm oil at the center of the pipe and the cold environment at the exterior. The higher the temperature difference the higher the potential that drives the diffusion. The wax molecules must not be precipitated already, but must be in solution with the bulk oil for the deposition to occur. Wax that is already precipitated when reaching the wall surface does not deposit.

In addition to the molecular diffusion, wax deposits are created by shear dispersion, gravity settling, Brownian diffusion and Soret diffusion. In case of turbulent flow, the wax deposition is less than that in laminar flow due to shear stripping (Sarica Cem, 2004). However, this phenomenon is too random and there are no published studies describing it mathematically as a function of flow speed or otherwise.

The wax deposition phenomenon is best described by the mechanism proposed by Singh et al. There are five distinct steps in the formation of wax deposition on pipelines (Probjot Singh R. V., Formation and Aging of Incipient Thin Film, 2000)

- Initially, crystals are created close to the relatively cold surface of the pipe wall. Macroscopically, the oil that is rich in crystals becomes an incipient gel layer tangent to the wall.
- Waxes with hydrocarbon number greater than the critical diffuse from the oil bulk towards the gel.
- Further diffusion of these molecules within the deposit through the oil that is still trapped in the deposit.
- Precipitation of the molecules in the deposit.
- At the same time, solvent molecules (oil particles with carbon number lower than the critical) are counter-diffused towards the center of the pipe. Gradually, the gel solidifies into a wax deposition attached to the wall.

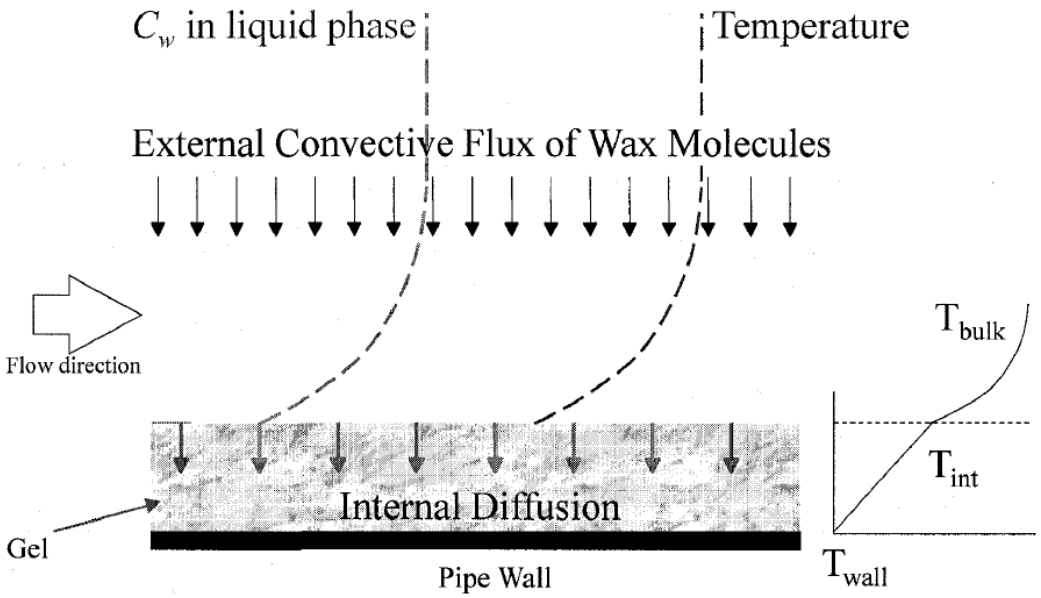


**Figure 5:** Schematic showing the wax deposition mechanism proposed by Singh et al **(P.Singh, 2000)**.

This phenomenon is called wax aging and as indicated above is a weak function of pressure and a strong function of the temperature gradient between the center of the pipe and the wall. During the wax deposit aging, the wax mass fraction increases while the oil mass fraction decreases. This results in the decrease of the thermal conductivity of the wax deposit whose contribution on the insulation of the pipe wall increases over time.

### 3.3. Experimental Setup Used by Singh et al (P.Singh, 2000).

This section describes the experiment upon which the wax deposition conclusions were drawn. The experimental setup is a flow loop with three distinct sections designed for better monitoring and control of the experiment (Figure 6). The first section includes a stirred vessel were the oil-wax mixture is poured. Its temperature is kept at 30°-35° C to prevent the wax from precipitating whilst stirring ensure the homogeneity of the mixture. After the tank, there is the pump that circulates the oil-wax mixture into the flow loop.

The test section exists within the walls of the loop which go through a cold-fluid tank and are kept at low temperature, way below the cloud point to enforce the wax precipitation and deposition. Pressure taps allow for monitoring the pressure drop along the test section, an indicator of the wax deposit thickness. The third section has similar pressure taps and functions as a reference for a wax-free pipe

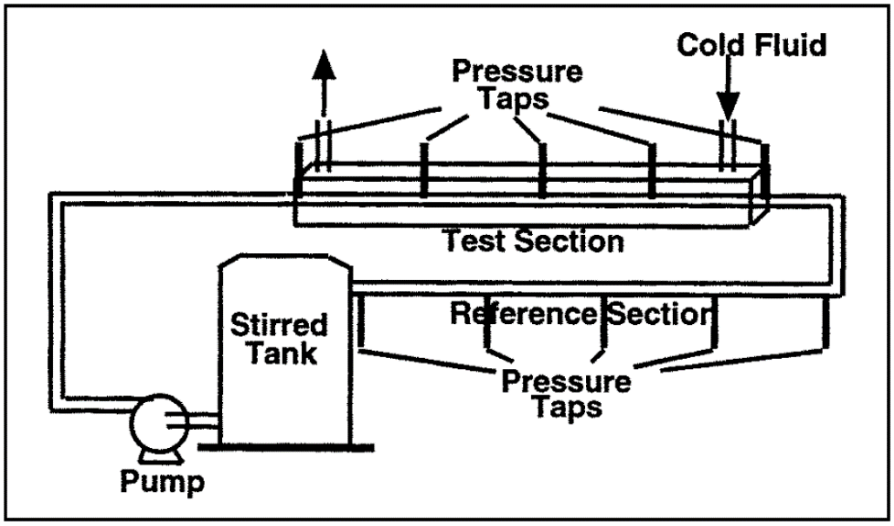


**Figure 6:** Flow loop used by Singh et al.

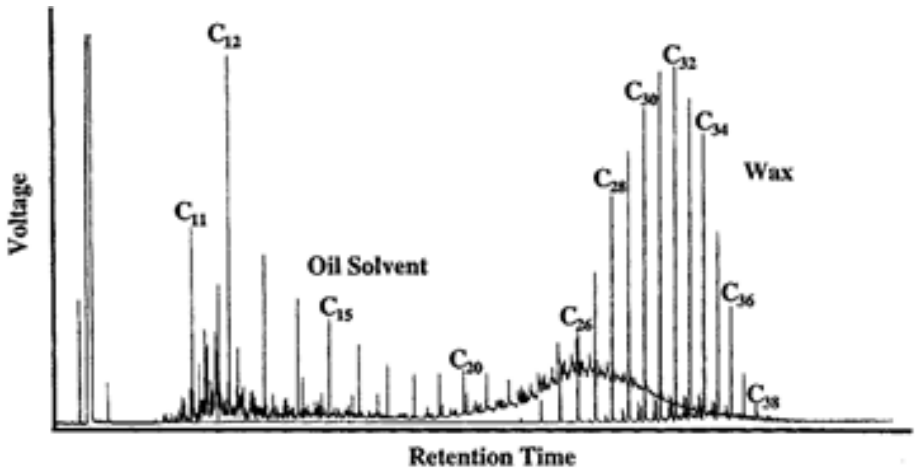


**Figure 7:** Chromatograms of the Singh et al. wax-oil mixture.

The fluid used to simulate the crude oil was a mixture of food grade wax (Mobil M140) and oil solvent. Its chromatographic profile is shown in Figure 3. Although it is unlike any natural crude oil mixture (Figure 4) it is still a continuous distribution of solvents. The advantage of having 'heavy' along with 'light' components is that it allows for better observation of the diffusion phenomenon, fundamental in the process of wax aging.

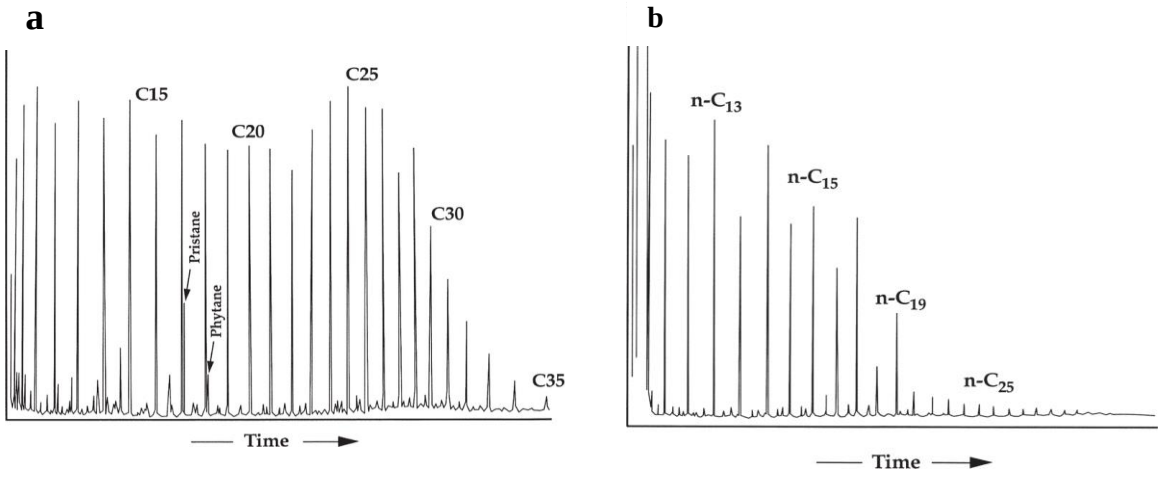


**Figure 8:** a) Chromatogram of oil rich in wax **(Robinson, 1987)** b) Chromatogram of oil poor in wax **(Hatch, 1990)**.

## 3.4. The Physics of the Wax Deposition Model

Singh et al. (P.Singh, 2000) identify five steps that occur towards the formation of the wax deposit. At an early stage, the low-temperature pipe walls are covered with a layer of oil and wax precipitates. This layer is initially in semi-solid form and is referred to as the incipient gel layer. When this gel solidifies due to aging there are three different layers, the wax deposit, the waxy gel layer and the flowing oil.

The next three steps are the diffusion of wax from the oil to the waxy gel, from the waxy gel to the wax deposit and then inside the wax deposit. The fifth step is counter-diffusion of lighter molecules (whose carbon number is lower than the critical).

According to Singh et al., there are other mechanisms, such as the Brownian diffusion, gravity settling and shear dispersion that play a role but only in the particulate deposition of wax. Their experimental results support that particulate deposition is insignificant in subsea pipelines and so their model does not include them.

The aging of the wax deposit is heavily dependent on the temperature gradient between the pipe wall and the oil bulk temperature. In the experiments of Singh et al. molecules with carbon number same as the critical would virtually not deposit at all if the temperature gradient was not big enough.

Finally, the pressure of the fluid exerts a compressive force radially towards the pipe wall. This further drives the aging of the wax deposit making it more rigid with time. Singh's team carried out experiments to determine the effect of pressure in the wax deposition. They run the same experiment with high and low temperature gradient and kept pressure the same. Wax deposition was almost non-existent for the low temperature gradient proving it to be the primary mechanism of solid wax built-up.

## 3.5. Assumptions and Verification

Singh et al. make the following assumptions in their model.

- The dominant mechanism is molecular diffusion. Singh et al. left the oil-wax mixture to cool below the cloud point wax particles were formed in the oil bulk. After turning on the circulation of the mixture and monitoring it for hours they found no wax deposition. In the case of a pipeline, at a distance from the well, this phenomenon further decreases the wax deposition rate.

- The shear removal is negligible. In the experiment where the particulate deposition was monitored, Singh et al monitored sloughing as well. For flow with Re < 2100 there was no sloughing whilst for Re = 5200 there was a negligible amount of shear removal. In the case of a pipeline, these particulates might only form away from the well.

- All processes are assumed to be quasi-steady state. This means that the heat transfer is instantaneous and that the axial heat transfer is neglected. When distributing the temperature of the bulk along the pipeline, this means that the higher the discretization, the more accurate the Singh et al. model will be. As discussed below, each segment has the same temperature at the entrance with that at the exit.

- The wax concentration in the thin gel layer does not vary radially. The wax layers examined by Singh et al are thin enough for this to hold true. In the case of a pipeline and a long term prediction a wax deposit might grow big enough for this assumption to be invalid. In this case, the existence of wax in the deposit makes the diffusion harder, thus the wax deposition rate might be overestimated when using the Singh et al. model.

- The thermal conductivity of the gel is a function of its wax content. In this study the thermal conductivity was held steady due to lack of data.

In addition to Singh et al. assumptions there is a phenomenon that is not clearly accounted for, that is the heat due to friction with the pipe wall. Initially it is negligible, but as the wax deposit increases in thickness the surface is not smooth anymore. The heat produced due to friction might increase locally the temperature gradient.

## 3.6. Problems Arising from Wax Deposition

Wax deposition has been a problem for the petroleum industry for many decades. The richer the oil in heavy components the more severe are the problems related to wax deposition. From a technical point of view, these issues are (Tao Zhu University of Alaska Fairbanks, 2008).

- Wax deposition around the wellbore and its vicinity reduces the permeability of the oil from the deposit orifice into the pipe.
- Gradual clogging and eventually plugging of the pipeline.
- Once the oil is in the reservoir it undergoes phase separation which changes the viscosity of the oil while wax is deposited at its wall.
- The wax deposit has a rougher surface than the pipe itself which, combined with the reduced diameter of the pipeline, exerts increased strain on the pumps.

In terms of cost, the above are translated into (Tao Zhu University of Alaska Fairbanks, 2008):

- Increased operating expenses of the whole system which may render it counter-productive and may lead to its shut-down.
- Limitation of production.
- The extra cost of pigging, direct electrical heating (DEH), chemical cleaning and other methods and managing wax in general jeopardizes the development of marginal fields. Depending on the concurrent oil price, wax deposition may lead to abandoning these fields.

## 3.7. The Effect of Temperature on Wax Deposition

There are two parameters heavily depending on temperature that define the wax deposition rate. These are the mass diffusivity $D_{wo}$ and effective $D_e$ and the wax solubility in the oil $C_{ws}$.

### 3.7.1. Diffusivity

Diffusivity expresses the rate by which molecules move through a surface of solvent ($m^2/s$) and the higher its value the easier for the solvent to move through. In the case of wax deposition, high diffusivity results in high deposition rate. The diffusivity equation for paraffins in paraffinic solvents is given by Hayduk and Minhas (Hayduk, 1982) with an average error of 3.4%.

$$D_{wo} = 13.3 \times 10^{-8} \times \frac{T^{1.47}\mu^{\gamma}}{V_A^{0.71}} \; {cm^2}/{s}\,, \tag{17}$$

where $T$ is the bulk oil temperature ($K$), μ is the solvent viscosity ($mPa\ s$), $V_A$ is the molar volume of the paraffin (cm3/mol), and γ is a function of $V_A$.

$$\gamma = \frac{10.2}{V_A} - 0.791\,. \tag{18}$$

In addition to the diffusivity of the wax in the bulk oil, there is also the diffusivity of the wax molecules in the wax deposit where there is still oil. This is called the effective diffusivity and is expressed as (Cussler, 1988).

$$D_e = \frac{D_{wo}}{1 + {\alpha^2 \bar{F}_w^2}/{(1 - \bar{F}_w)}}\,, \tag{19}$$

where the greek α stands for the average aspect ratio of the wax crystals and $\bar{F}_w$ is the mass fraction of wax in the deposit. This expression is derived for porous medis of flake-like particles and is

dependent on the temperature that is between the oil-wax interface and the ambient temperature. The temperature calculation in given by section 0.

### 3.7.2. Solubility of Wax in Solvent

Solubility expresses the maximum density of wax that can be dissolved in the oil and be in one phase with it. Note that the wax not dissolved does not necessarily precipitate, it may still be in liquid phase but not soluble. As mentioned in the literature (Creek, 1999) (P.Singh, 2000), wax molecules diffuse into the deposit both from the pool of dissolved wax and the wax that is not soluble.

Singh et al. provide an expression of the solubility of wax in oil solvent which is a strong function of temperature:

$$C_{ws}(T_i) = a\,(T_i + b)^c\,, \tag{20}$$

where $T_i$ is the oil-wax deposit interface temperature and *a,b,c* are coefficients unique for each pair of oil-wax mixture. In this study, due to lack of data, the values used for *a,b,c* are the same used by Singh et al. (P.Singh, 2000): $a = 4.9 \times 10^{-9}\ kg/m^3$ , $b = 17.8\ °C$, $c = 6\ °C$.

## 3.8. Lumped Parameter Model for Heat Transfer in a Pipeline

The temperature distribution of the bulk oil calculated in this way is a prerequisite for the viscosity calculation used to define the flow. In the following section a model is developed for temperature distribution of flowing crude oil inside a pipeline. Once the flow is determined, a more higher discretization is used to obtain the temperature profile for the wax concentration calculation.

### 3.8.1. Steady State Transfer of Heat in Pipelines

The subsea pipelines consist of layers of materials specialized for protection against galvanic erosion, for heat insulation and for strength. The heat flux from the oil bulk to the subsea environment through these layers is conductive in nature. The heat flux from the oil bulk to the pipe interior wall and from the pipe exterior wall to the sea water is convective. All these are thermal resistances which, for given bulk oil and sea water temperatures, define the heat flux which is expressed as:

$$q(x) = \frac{T_{oil}(x) - T_{sea\ water}}{\sum_{i=1}^{N} R_i}. \tag{21}$$

For a small pipe segment the above equation can be written as

$$dq(x) = UdA(T_{oil}(x) - T_{sea\ water})$$
$$or \tag{22}$$
$$dq(x) = U(\pi\ ID\ dx)(T_{oil}(x) - T_{sea\ water}),$$

where,

$$U^{-1} = ID \times \sum \left\{ \frac{\ln\left(\frac{ID_{n+1}}{ID_n}\right)}{2k_{cond_n}^{material}} \right\} + \frac{1}{h_i} + \frac{1}{h_0 \times \frac{OD}{ID}}. \tag{23}$$

This radial heat flux along the length of a pipe segment can also be expressed as the enthalpy drop of the oil bulk along that pipe segment:

$$dq(x) = -\dot{m}\, C_p\, dT_{oil}(x)$$

*or*

$$dq(x) = -\dot{m}\, C_p\, d(T_{oil}(x) - T_{sea\ water})\,. \tag{24}$$

Equating the expressions (22) and (24) yields

$$U\ \pi\ ID\ dx = -\frac{\dot{m}\ C_p\ d(T_{oil}(x) - T_{sea\ water})}{T_{oil}(x) - T_{sea\ water}}\,. \tag{25}$$

Integrating along the pipe length L

$$-\frac{U\ \pi\ ID\ L}{\dot{m}\ C_p} = ln(T_{oil}(x) - T_{sea\ water})|_0^L$$

*or*

$$T(L) = (T(0) - T_{sea\ water})e^{-\frac{U\ \pi\ ID\ L}{\dot{m}\ C_p}} + T_{sea\ water}\,. \tag{26}$$

### 3.8.2. Parameter Calculations

The internal convective heat transfer coefficient is given by

$$h_i = \frac{k_{cond}^{oil} Nu}{ID}. \tag{27}$$

The external convective heat transfer coefficient is given by

for unburied Pipeline

$$h_o = \frac{k_{cond}^{sea\ water} \times 0.52 \times Re^{0.6}}{OD}$$

for buried Pipeline

$$h_o = \frac{2 \times k_{cond}^{soil}}{OD \times cosh\left(\frac{2\,H}{OD}\right)}\,, \tag{28}$$

where H is the height from the seabed to the center of the pipeline.

The Nusselt number in equation (27) is given by

$$\begin{array}{ll} \text{for Laminar flow (Re<2300)} & \mathrm{Nu} = 3.66 + \dfrac{0.065\, Re \,\mathrm{Pr}\dfrac{ID}{L}}{1 + 0.04\left(Re\,\mathrm{Pr}\dfrac{ID}{L}\right)^{\frac{2}{3}}} \\ \text{for Turbulent flow (Re>10000) According to Dittus} & \mathrm{Nu} = 0.023\, Re^{4/5}\, Pr^{n}\,, \quad \begin{matrix} n=0.4\ for\ T_{solid}>T_{medium} \\ n=0.3\ for\ T_{solid}<T_{medium} \end{matrix}. \end{array} \tag{29}$$

The Reynolds number in equation (28) is given by

$$Re = \frac{\rho U_{\infty} OD}{\mu}, \tag{30}$$

where, ρ the sea water density in (*kg/m3*), $U_{\infty}$ the undisturbed uniform crossflow velocity (*m/s*) and $\mu$ the dynamic viscosity of the seawater (*Pa s*).

### 3.8.3. Pipe Segmentation and Temperature Distribution

The code calculating the temperature distribution according the equations (21) - (30) was applied successfully for a 3000 m pipeline. Then, the pipe was segmented and the same calculations were run for each segment. In either case, the temperature profile was exactly the same.

The equations above do not account for the latent heat due to solidification. However, the error in this assumption is very small. This is supported by the following rough calculation

Assume that a wax deposit of 1 cm is built up in an hour for a pipeline of 30cm in diameter (which is too big to be real). The latent heat of this mass is about 1880 kJ. For an oil flow of 89 kg/m3 through that pipe and an average oil temperature drop of 0.03°C/m along its length, the heat lost in an hour is 773,000 kJ. So, neglecting the solidification latent heat does not have any substantial effect in the temperature distribution calculation.

The segmentation is set according to the needs of the wax deposition model. However, it may also include variations like an area where the pipeline is buried or a subsea stream at a certain spot.

## 3.9. The Independent Heat and Mass Transfer Correlation, the Solubility Method and Bounds on the Wax Deposition Rate Calculation

The Seider –Tate formulation uses an independent heat-mass transfer correlation. It focuses on the *Sherwood* number *Sh*, which expresses the ratio of convective to diffusive mass transfer. In laminar flows the radial mass transfer is the diffusion of wax molecules and the axial is convective mass transfer. Thus, the *Sh* number can be used to find the mass of wax diffused toward the wall, given the overall mass transfer rate. For turbulent flows the *Sh* number can be found by the Chilton-Colburn analogy, a correlation similar that of Seider-Tate.

However, that method is that it deals the heat and mass transfer independently. The problem that arises with that is that with the transfer of heat, the temperature around wax molecules drops below the cloud point and that results in precipitation of wax. Once precipitated, the wax particles do not diffuse any more but are transferred convectively. So, counting this amount of wax as diffused is a mistake which is not insignificant (R.Venkatesan, 2004). Thus, the methodology above, proposed originally by Singh et al., is known as Independent Heat and Mass Transfer (IHMT) correlations lead to a maximum estimation of the wax deposition rate (Z.Huang, 2011).

The Solubility Method proposed by Venkatesan and Fogler (R.Venkatesan, 2004) accounts for the precipitated molecules but overestimates the amount of precipitated wax, some of which might be still in liquid phase and able to deposit. Thus, it results in a minimum calculation of wax deposition rate.

Shown in Figure 9 is the Schematic of Hyun Su Lee (Z.Huang, 2011) showing the wax radial distribution on a pipe. There is the solubility curve following the temperature distribution curve and beyond that starts the Super-Saturated area where the wax is no longer in solution with the oil but is still not precipitated. The solubility method follows the solubility curve (Cws) according to which very little wax precipitating in the oil bulk makes to the wall deposit. The Singh et al approach follows the Colburn Analogy according to which the wax precipitation increases greatly close to the wall which although true for laminar flows is not accurate for turbulent. Finally, the IHMT method estimates a wax profile that is restricted to the left of the Chilton-Colburn analogy curve and inside the Super-Saturated area. This method gives accurate results for both laminar and turbulent flow regimes.

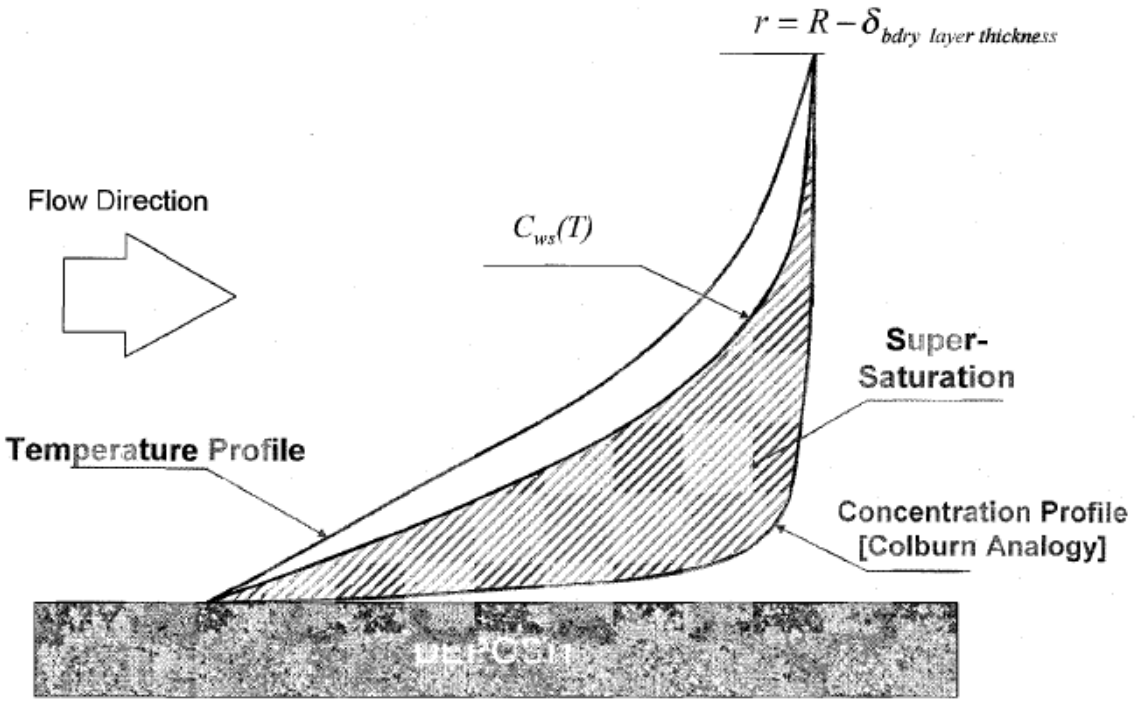


**Figure 9:** Axial wax concentration distribution of different methods. **(Z.Huang, 2011)**

## 3.10. Gas-Liquid Flow

The crude oil is usually a 2-phase mix of oil and gas. The flow of the mix changes depending on the gas volume fraction of the crude oil, pressure and temperature.

### 3.10.1. The Effect of Flow on Wax Deposition

There are two characteristics of the flow that affect the wax deposition rate, the flow rate $Q$ ($m^3/s$) and the flow type defined by the Reynolds number. Apparently, the higher the flow rate the higher the mass of wax moving through the pipeline and so the more increased the wax deposition rate. The flow rate is affected by the viscous losses which partially depend on the fluid viscosity and so the flow rate is tied to the temperature by which the viscosity changes significantly.

Regarding the flow type (*Re* number), it determines the transportation of heat and mass (*Nu* and *Sh* numbers), which in turn determine the amount of wax diffused towards the wax deposit.

### 3.10.2. Gas-Liquid Flow Regimes Description

The crude oil contains dissolved gas which under certain conditions separates from the bulk of the oil making the flow in the pipeline a two-phase flow. Depending on the pressure, the gas concentration in the oil, the pressure difference at the ends of the pipeline which drives the flow, the oil and gas viscosity and density, the flow patterns change. There are six distinct flow regimes though, the Dispersed Bubble Flow, the Stratified Flow, the Stratified Wavy Flow, the Annular-mist Flow, the Bubble Flow and the Intermittent Flow (Bratland, 2010). Knowing the flow speed of gas and liquid these regimes can be approximately mapped in five different areas on a system where the horizontal axis represents the superficial gas velocity and the vertical the superficial liquid velocity.

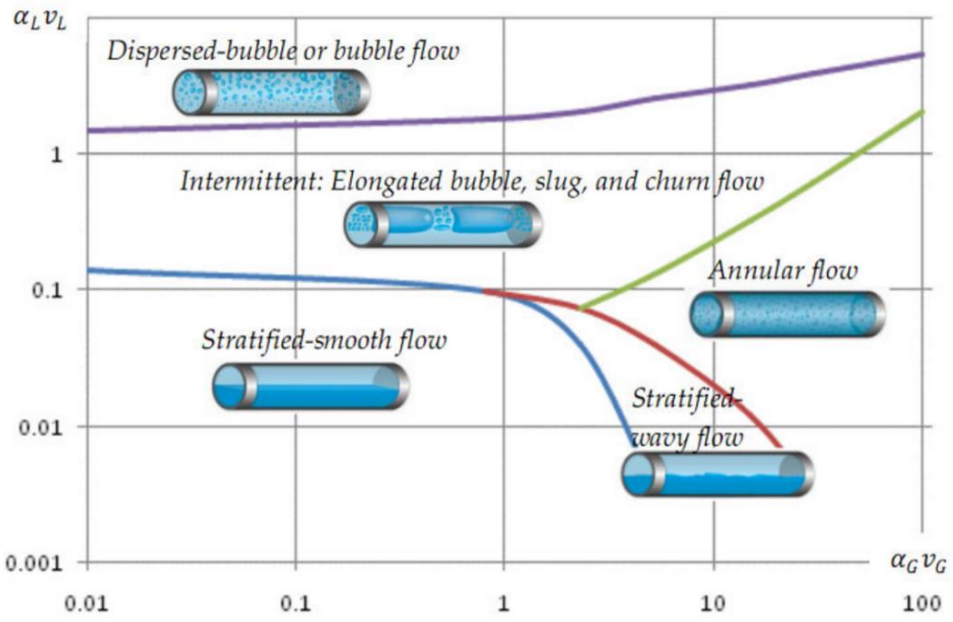


**Figure 10:** Flow regimes depiction in relation to the gas and liquid superficial velocities. **(Bratland, 2010)**

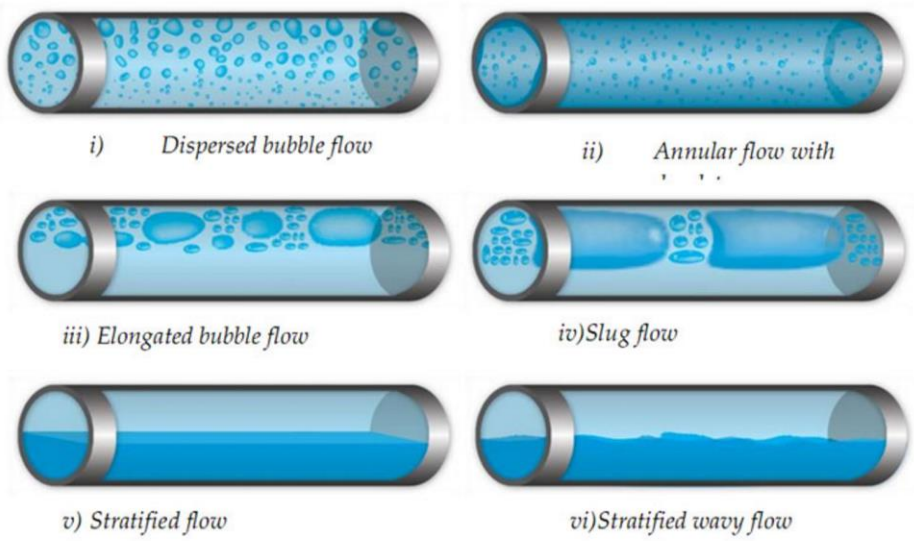


**Figure 11:** Flow regimes depiction. **(Bratland, 2010)**

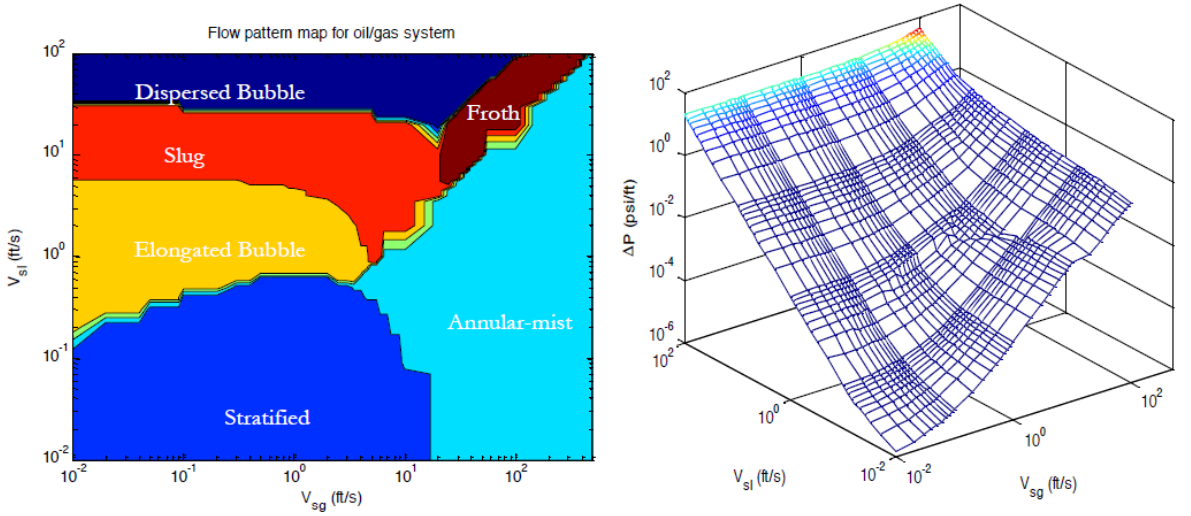


Flow pattern map for a horizontal Pipe

Pressure gradient for oil-gas system for different liquid and gas velocities

**Figure 12:** Flow regimes mapping and 3D mapping for steady-state pressure drop. *Courtesy of the University of Houston.*

For low liquid and gas superficial velocities the flow is smooth, like the slow flow on a wide river. As the gas speed increases it causes ripples on the surface of the liquid due to tensional stresses. The stratified flow covers the two areas at the bottom of the mapping (Figure 10), where the liquid speed is low. Further increasing the gas speed drives the flow into the annular regime where the gas flow is high enough to cause turbulence in the liquid due to tension.

When increasing the liquid speed, the flow enters the intermittent regime where the gas forms big bubbles that tend to float at the top section of the pipe. Due to their compressibility these slugs cause unwanted pressure variations. Their cause of creation is either hydrodynamic or terrain. In the second case the path of the pipeline follows a zig-zag elevation where the liquid tends to plug the lower flow section until enough pressure builds up in the gas to escape (Figure 13).

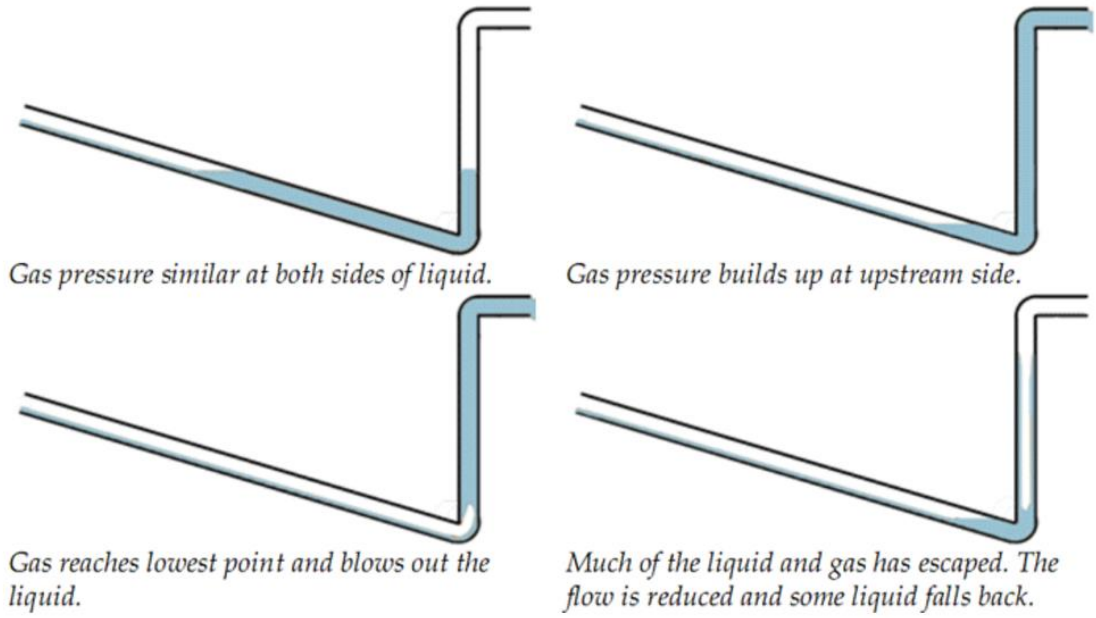


**Figure 13:** Terrain generation of slugs. **(Bratland, 2010)**

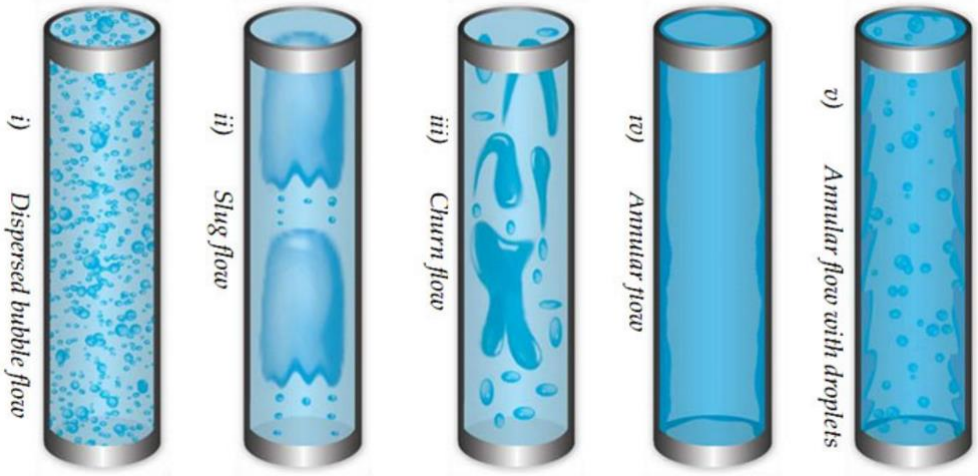


**Figure 14:** Flow regimes in vertical pipes **(Bratland, 2010)**

In this study, the flow is considered steady and so it has to assume that the pipeline lies on a flat seabed.

For each oil sample the mapping is different as the viscosity and density of the gas mixture and those of the oil mixture are different. In the following section, a model is described with which the flow regime can be accurately defined.

### 3.10.3. The Mechanistic Model and the Beggs and Brill Correlation.

As early as 1976 (Y.Taitel, 1976) there has been a research effort to make a model by which the flow regimes of an oil sample can be predicted. The *mechanistic model* of Yemada and Dukler for horizontal pipe lines was expanded by Aziz and Petalas (N. Petalas, 2000) to include the inclination. That means that the flow regime of a vertical pipeline (Figure 14) can be described as well. The algorithm for defining the flow regime by use of the mechanistic model is elaborate and has many conditions (Figure 15).

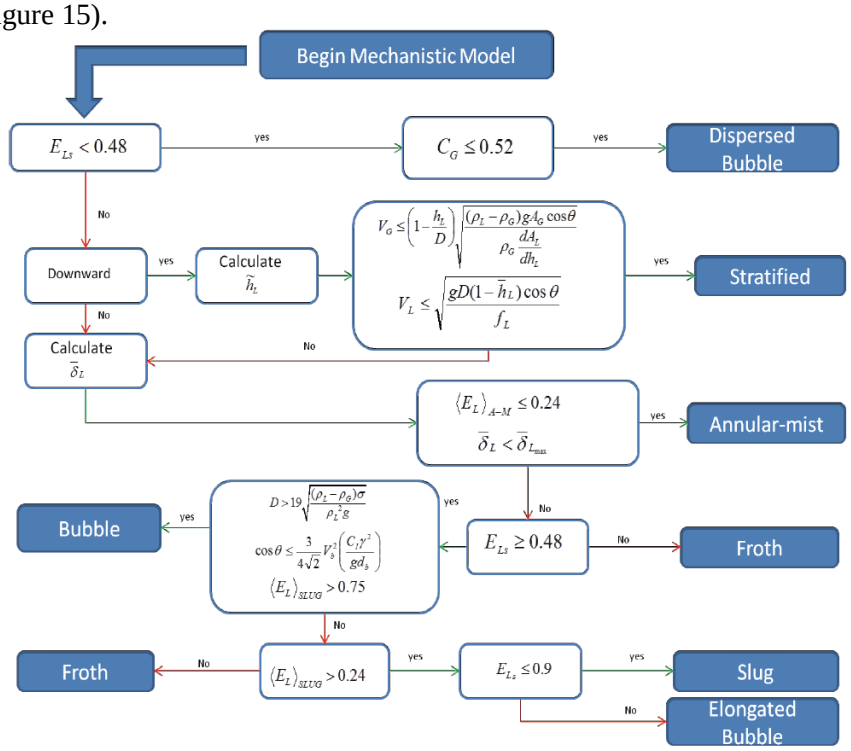


**Figure 15:** Flow chart for the determination of the flow regime using the Mechanistic Model of Aziz-Petalas. **(A.Meziou, 2016)**

The algorithm of Figure 15 can be simplified by using the Beggs and Brill correlation which relates the no-slip Darcy friction factor of a liquid-gas flow with the equivalent two phase friction factor. This is the algorithm finally used in this thesis and it is described in the next section.

### 3.10.4. The Beggs and Brill Correlation

This section presents the algorithm with which the flow regime is determined (N. Petalas, 2000).

- Determination of the Froude number is given by:

$$Fr = \frac{Inertia}{Gravity} = \frac{{V_m}^2}{gD}. \tag{31}$$

- Non-Slip Liquid Holdup is given by:

$$E_{SL} = \frac{V_{SL}}{V_m} = \frac{Q_L}{Q_L + Q_G}. \tag{32}$$

- Non-Dimensional numbers is given by:

$$L_1 = 316\ {E_{SL}}^{0.302}, \qquad L_2 = 0.0009252\ {E_{SL}}^{-2.4684},$$
$$L_3 = 0.1\ {E_{SL}}^{-1.4516}, \qquad L_4 = 0.5\ {E_{SL}}^{-6.738}. \tag{33}$$

- Flow regime limits are given by:

for segregated flow
$$E_{SL} < 0.01 \quad and \quad Fr < L_1$$
$$or$$
$$E_{SL} \geq 0.01 \quad and \quad Fr < L_2,$$

for transitional flow
$$E_{SL} \geq 0.01 \quad and \quad L_2 < Fr < L_2,$$

for intermittent floe
$$0.01 \leq E_{SL} < 0.4 \quad and \quad L_3 < Fr \leq L_1$$
$$or \tag{34}$$
$$E_{SL} \geq 0.4 \quad and \quad L_3 < Fr < L_4,$$

for distributed flow $E_{SL} < 0.4 \quad and \quad Fr \geq L_1$

*or*

$E_{SL} \geq 0.4 \quad and \quad Fr < L_4$ .

- The liquid holdup calculation is calculated as

$$E_L = \frac{aE_{SL}^b}{Fr^c}, \tag{35}$$

where a,b,c are given by **Table 1**.

**Table 1:** Pipe Insulating Materials

| | **a** | **b** | **c** |
|---|---|---|---|
| **Segregated Flow** | 0.98 | 0.4846 | 0.0868 |
| **Intermittent Flow** | 0.845 | 0.5351 | 0.0173 |
| **Distributed Flow** | 1.065 | 0.5824 | 0.0609 |

- The Liquid holdup calculation for Transition Flow is given by:

$$E_{L_{Trans}} = \kappa E_{L_{Seg}} + (1-\kappa)E_{L_{Int}} \; ; \; \kappa = \frac{L_3 - Fr}{L_3 - L_2}. \tag{36}$$

- The calculation of the no-slip density is given by:

$$\rho_n = E_{SL}\rho_L + (1 - E_{SL})\rho_G \, . \tag{37}$$

- The calculation of the no-slip viscosity is given by:

$$\mu_n = E_{SL}\mu_L + (1 - E_{SL})\mu_G \, . \tag{38}$$

- The calculation of the no-slip Reynold's number is given by:

$$Re_n = \frac{\rho_n V_m \, ID}{\mu_n} \, . \tag{39}$$

- The calculation of the no-slip Darcy friction factor is given by:

$$\begin{cases} f_n = \dfrac{64}{Re_n} & \begin{matrix} Laminar\ Flow \\ Re < 2300 \end{matrix} \\ f_n = \dfrac{0.316}{{Re_n}^{0.25}} & \begin{matrix} Turbulent\ Flow \\ Re > 2300 \end{matrix} \end{cases}. \tag{40}$$

- The calculation of parameter y is given by:

$$y = \frac{E_{SL}}{{E_L}^2}. \tag{41}$$

- The calculation of the Beggs and Brill correlation parameter s is:

$$\begin{cases} s = \dfrac{\ln(2.2x - 1.2)}{\ln(y)} & 1<y\leq 1.2 \\ s = \dfrac{\ln(y)}{-0.0523+3.182\ln(y)-0.8725\ln(y)^2+0.01853\ln(y)^4} & y\leq 1\ or\ y>1.2 \end{cases}. \tag{42}$$

- The calculation of the two-phase friction factor (Beggs and Brill Correlation) is:

$$f_{tp} = f_n \exp(s). \tag{43}$$

- The calculation of the friction loss term is given by:

$$\Delta P_f = \frac{f_{tp}\rho_n V_m^2}{2D}. \tag{44}$$

- The equivalent bulk modulus is calculated as:

$$\frac{1}{\beta_{eq}} = \frac{E_L}{\beta_L} + \frac{1-E_L}{\beta_G}. \tag{45}$$

- The equivalent density at atmospheric pressure is given by:

$${\rho^0}_{eq} = E_L\rho_L^0 + (1 - E_L)\rho_G^0. \tag{46}$$

- The equivalent density after taking into account the effect of fluid compressibility is given by:

$$\rho_{eq}(P) = {\rho^0}_{eq}\left(1 + \frac{1}{\beta_{eq}}(P - P_0)\right). \tag{47}$$

- The equivalent speed of sound in the fluid (not used in this study) is calculated as:

$$c_{eq} = \sqrt{\frac{\beta_{eq}}{\rho_{eq}}}. \tag{48}$$

- For the equivalent viscosity the calculation is:

$$\begin{cases} \mu_{eq} = \dfrac{\rho_{eq}}{\rho_n}\mu_n \exp(s) & \begin{matrix} Laminar\ Flow \\ Re < 2300 \end{matrix} \\ \mu_{eq} = \dfrac{\rho_{eq}}{\rho_n}\mu_n \exp(4s) & \begin{matrix} Turbulent\ Flow \\ Re > 2300 \end{matrix} \end{cases}. \tag{49}$$

- Finally, the two-phase Reynolds number calculation is given by:

$$Re_{tp} = \frac{\rho_{eq} V_m D}{\mu_{eq}} \tag{50}$$

## 3.11. Heat and mass Transfer Computation

The heat transfer affects the axial temperature profile along the pipe which in turn defines the precipitation in the oil bulk and at the wall. In turn, the amount of wax precipitated at the wall creates a layer of insulation that changes the temperature profile. The heat and mass transfer are entwined together.

### 3.11.1. The *Sh* and *Nu* Computation.

The wax deposition rate is strongly related to the solubility and the diffusion rate, both of which depend on the temperature. Also, the wax deposition rate is directly connected to the wax concentration in the bulk oil. Thus, it is important to have precise calculations for the temperature and the wax concentration profiles near the interface of the oil-wax deposit. From these the numbers defining the heat and mass transfer, *Nu* and *Sh* respectively, are calculated. In this study, the method used to calculate the *Nu* and *Sh* is the computational approach proposed by Hyun Su Lee (Lee, 2008) where the *Nu* and *Sh* are given by

$$Nu = \frac{(-2r_i)\left.\frac{\partial T}{\partial r}\right|_{r=r_i}}{T_b - T_i} = \frac{2r_i h_i}{k_{cond}^{oil}} \tag{51}$$

and

$$Sh = \frac{(-2r_i)\left.\frac{\partial C}{\partial r}\right|_{r=r_i}}{C_b - C_i} = \frac{2r_i k_M}{D_{wo}}, \tag{52}$$

where $k_{cond}^{oil}$ is the thermal conductivity coefficient of the oil, $k_M$ is the mass transfer coefficient, $\left.\frac{\partial T}{\partial r}\right|_{r=r_i}$, $\left.\frac{\partial C}{\partial r}\right|_{r=r_i}$ the temperature and wax concentration gradients at the oil-wax deposit interface, $T_{b,i}$ , $C_{b,i}$ the temperature and wax concentration of the bulk oil at the center of the pipeline ($_b$) and at the interface ($_i$).

### 3.11.2. Heat and Mass Transfer Equations for Laminar Flow and Boundary Conditions

The temperature and the wax concentration profiles, in explanation the radial distributions of temperature and wax concentration, can be calculated by solving the following energy balance and mass balance equations

Mass Transfer $$v_z \frac{\partial C}{\partial z} = \frac{1}{r}\frac{\partial}{\partial r}\left[rD_{wo}\frac{\partial C}{\partial r}\right] - k_r(C - C_{ws}), \quad (53)$$

where $\frac{\partial C}{\partial z}$ is the axial wax concentration gradient, $\frac{\partial}{\partial r}$ is the radial gradient, $C$ is the wax concentration and $C_{ws}$ is the solubility, $k_r$ is the precipitation rate constant and $v_z$ is the velocity.

The left hand side of (53) expresses the change of mass along the pipeline. Any variation in the axial direction occurs due to wax depositing at the wall by diffusion. The first term on the right hand side expresses the radial diffusive mass transfer. Of the molecules diffused toward the wall however, not all deposit but some precipitate. The precipitation is expressed by the second term. (see section 3.11.5).

Heat Transfer $$v_z \frac{\partial T}{\partial z} = \frac{1}{r}\frac{\partial}{\partial r}\left[ra_T\frac{\partial T}{\partial r}\right] - \beta(C - C_{ws}), \quad (54)$$

where $\frac{\partial T}{\partial z}$ is the axial gradient, $\frac{\partial}{\partial r}$ is the radial gradient, $C$ is the wax concentration and $C_{ws}$ is the solubility, $v_z$ is the velocity, $\beta = \frac{k_r \Delta H_f}{\rho C_p}$ and $a_T = \frac{k_{cond}^{oil}}{\rho C_p}$ is the thermal diffusivity.

The left hand side of equation (54) expresses the change of mass along the pipeline. The first term on the right hand side is the radial variation of temperature due to conductivity. The second term expresses the alteration in temperature due to the solidification heat of the precipitated wax. However, this term is insignificant (less than 0.1%) and can be neglected (Lee, 2008). Thus, the energy balance can be written as:

Heat Transfer $$v_z \frac{\partial T}{\partial z} = \frac{1}{r}\frac{\partial}{\partial r}\left[r a_T \frac{\partial T}{\partial r}\right] \quad (54)$$

For both the energy and mass balance equations the velocity profile is parabolic and is expressed as

$$v_z = 2v_{avg}\left[1 - \left({}^{r}/_{r_i}\right)^2\right], \quad (55)$$

where $r_i$ is the radius at the interface.

The boundary conditions for (53) and (54) are set as (Lee, 2008)

$$\begin{cases} C = C_b & at\ z = 0 \\ \frac{\partial C}{\partial r} = 0 & at\ r = 0 \\ C = C_{ws}(T_i) & at\ r = r_i \\ C = C_{wall} = C_{ws}(T_{wall}) & at\ r = R \end{cases} \quad and \quad (56)$$

$$\begin{cases} T = T_b & at\ z = 0 \\ \frac{\partial T}{\partial r} = 0 & at\ r = 0. \\ T = T_{wall} & at\ r = R \end{cases} \quad (57)$$

The wax concentration at the oi-wax deposit interface ($C = C_{wall} = C_{ws}(T_{wall})$) is in *thermodynamic equilibrium* (Lee, 2008), a condition demanding no ambivalence regarding the thermodynamic condition of the wax, solid or liquid. Thus, all supersaturated wax molecules deposit at that point as they precipitate and all wax, that is still soluble in the oil within the deposit, follows the solubility curve $C_{ws}$.

### 3.11.3. Heat and Mass Transfer Equations Discretization.

The discretization scheme for the mass and heat transfer equations is the same as the one used is Lee's study (Oosthuizen, 1999). The mass transfer equation (53) is discretized as

$$A_j^c C_{ij} + B_j^c C_{ij+1} + C_j^c C_{ij-1} = D_j^c \,, \tag{58}$$

where

$$A_j^c = \frac{v_{z,j}}{\Delta z_i} + \frac{1}{r_j}\frac{2}{\Delta r_{j+1} + \Delta r_j}\left\{\left[\frac{r_{j+1}D_{wo,j+1} + r_j D_{wo,j}}{2}\right]\frac{1}{\Delta r_{j+1}} + \left[\frac{r_j D_{wo,j} + r_{j-1}D_{wo,j-1}}{2}\right]\frac{1}{\Delta r_j}\right\}$$

$$+ k_r$$

$$B_j^c = \frac{1}{r_j}\frac{2}{\Delta r_{j+1} + \Delta r_j}\left\{\left[\frac{r_{j+1}D_{wo,j+1} + r_j D_{wo,j}}{2}\right]\frac{1}{\Delta r_{j+1}}\right\}$$

$$C_j^c = \frac{1}{r_j}\frac{2}{\Delta r_{j+1} + \Delta r_j}\left\{\left[\frac{r_j D_{wo,j} + r_{j-1}D_{wo,j-1}}{2}\right]\frac{1}{\Delta r_j}\right\}$$

$$D_j^c = \frac{v_{z,j}C_{i-1j}}{\Delta z_i} + k_r C_{ws}(T_{ij}) \,.$$

Equation (58) and the wax concentration boundary conditions can be written in matrix form as

$$\begin{bmatrix} 1 & -1 & 0 & 0 & 0 & \cdots & 0 & 0 & 0 \\ C_2^c & A_2^c & B_2^c & 0 & 0 & \cdots & 0 & 0 & 0 \\ 0 & C_3^c & A_3^c & B_3^c & 0 & \cdots & 0 & 0 & 0 \\ 0 & 0 & C_4^c & A_4^c & B_4^c & \cdots & 0 & 0 & 0 \\ \vdots & \vdots & \vdots & \vdots & \vdots & \ddots & \vdots & \vdots & \vdots \\ 0 & 0 & 0 & 0 & 0 & \cdots & C_{NFLUID-1}^c & A_{NFLUID-1}^c & B_{NFLUID-1}^c \\ 0 & 0 & 0 & 0 & 0 & 0 & 0 & 0 & 1 \end{bmatrix} \begin{bmatrix} C_{i1} \\ C_{i2} \\ C_{i3} \\ C_{i4} \\ \vdots \\ C_{iNFLUID-1} \\ C_{iNFLUID} \end{bmatrix} = \tag{59}$$

$$\begin{bmatrix} D_1^c \\ D_2^c \\ D_3^c \\ D_4^c \\ \vdots \\ D_{NFLUID-1}^c \\ C_{ws}(T_i) \end{bmatrix}.$$

The NFLUID node in (59) coincides with the oil-wax deposit interface. As mentioned in section 3.11.2, beyond the interface and within the wax deposit, the wax concentration is given solely by the solubility function. The heat transfer equation is expressed as:

$$A_j^t C_{ij} + B_j^t C_{ij+1} + C_j^t C_{ij-1} = D_j^t \tag{60}$$

where,

$$A_j^t = \frac{v_{z,j}}{\Delta z_i} + \frac{1}{r_j}\frac{2}{\Delta r_{j+1} + \Delta r_j}\left\{\left[\frac{r_{j+1}\alpha_{T,j+1} + r_j\alpha_{T,j}}{2}\right]\frac{1}{\Delta r_{j+1}} + \left[\frac{r_j\alpha_{T,j} + r_{j-1}\alpha_{T,j-1}}{2}\right]\frac{1}{\Delta r_j}\right\} + k_r$$

$$B_j^t = \frac{1}{r_j}\frac{2}{\Delta r_{j+1} + \Delta r_j}\left\{\left[\frac{r_{j+1}\alpha_{T,j+1} + r_j\alpha_{T,j}}{2}\right]\frac{1}{\Delta r_{j+1}}\right\}$$

$$C_j^t = \frac{1}{r_j}\frac{2}{\Delta r_{j+1} + \Delta r_j}\left\{\left[\frac{r_j\alpha_{T,j} + r_{j-1}\alpha_{T,j-1}}{2}\right]\frac{1}{\Delta r_j}\right\}$$

$$D_j^t = \frac{v_{z,j}T_{i-1j}}{\Delta z_i}.$$

In (Lee, 2008) the matrix corresponding to the heat transfer balance and the temperature boundary conditions is written in a similar way as the mass balance matrix and boundary conditions. Here, for elaboration, this matrix is expanded to include the heat transfer balance from the interface to the pipe exterior.

The interface temperature is no longer given by the ambient temperature, but by the convection equation (in matrix form):

$$\begin{bmatrix}1 & -1\end{bmatrix}\begin{bmatrix}T_{NFLUID-1}\\ T_{NFLUID}\end{bmatrix} = \frac{q}{h_i A}, \tag{61}$$

where q is the heat flux, $h_i$ the convection coefficient and $A$ the surface, which is given as

$$A = 2\pi R_j\, dz\,. \tag{62}$$

The heat flux q is calculated as

$$q = \pi\, ID\; dz\; \frac{\Delta T}{dr} \frac{1}{\frac{1}{h_i \pi ID} + \frac{1}{h_o \pi OD} + dz \sum_{n=1}^{Nins} \frac{\delta(n)}{k_{cond}^{layer}(n) \pi D(n)}}\ , \tag{63}$$

where $\delta(n)$ is the thickness of each $n$ layer, $k_{cond}^{layer}(n)$ the conductivity coefficient for the respective layer and $D(n)$ the diameter. $ID$ is the Inside Diameter and $OD$ is the Outside Diameter.

In addition to the equation (61), the conductive and convective equations, in matrix form are as follows:

$$\begin{array}{ll} \text{Conduction terms} & [1 \quad -1] \begin{bmatrix} T_{j-1} \\ T_j \end{bmatrix} = \frac{q}{k_{cond\ j}^{layer} A} \\ \text{External convection term} & [1 \quad -1] \begin{bmatrix} T_{N-2} \\ T_{N-1} \end{bmatrix} = \frac{q}{h_{out} A} \\ \text{Boundary Condition} & [0 \quad 1] \begin{bmatrix} T_{N-1} \\ T_N \end{bmatrix} = T_{ambient}\ . \end{array} \tag{64}$$

Finally, the heat balance matrix system is formulated as

$$\begin{bmatrix} 1 & -1 & 0 & 0 & 0 & \cdots & 0 & 0 & 0 \\ C_2^t & A_2^t & B_2^t & 0 & 0 & \cdots & 0 & 0 & 0 \\ 0 & C_3^t & A_3^t & B_3^t & 0 & \cdots & 0 & 0 & 0 \\ 0 & 0 & C_4^t & A_4^t & B_4^t & \cdots & 0 & 0 & 0 \\ \vdots & \vdots & \vdots & \vdots & \vdots & \ddots & \vdots & \vdots & \vdots \\ 0 & 0 & 0 & 0 & 0 & \cdots & C_{NFLUID-1}^t & A_{NFLUID-1}^t & B_{NFLUID-1}^t \\ 0 & 0 & 0 & 0 & 0 & 0 & 0 & 1 & -1 \\ 0 & 0 & 0 & 0 & 0 & 0 & 0 & 1 & -1 \\ 0 & 0 & 0 & 0 & 0 & 0 & 0 & \ddots & \vdots \\ 0 & 0 & 0 & 0 & 0 & 0 & 0 & 1 & -1 \\ 0 & 0 & 0 & 0 & 0 & 0 & 0 & 0 & 1 \end{bmatrix} \begin{bmatrix} T_{i1} \\ T_{i2} \\ T_{i3} \\ T_{i4} \\ \vdots \\ T_{iNFLUID-1} \\ T_{iNFLUID} \\ T_{iNFLUID+1} \\ \vdots \\ T_{N-1} \\ T_N \end{bmatrix} = \begin{bmatrix} D_1^t \\ D_2^t \\ D_3^t \\ D_4^t \\ \vdots \\ D_{NFLUID-1}^t \\ q/h_i A \\ q/k_{cond\ j}^{layer} A \\ \vdots \\ q/h_{out} A \\ T_{ambient} \end{bmatrix}, \quad (65)$$

where N is the total number of nodes counting from the center of the pipeline to the outmost point of the exterior wall. The heat balance equation (65) is solved first and using the calculated temperature profile on each axial node the wax concentration profile is calculated form the mass balance equation (59).

### 3.11.4. Heat and mass Transfer Equations for Turbulent Flow and Boundary Conditions.

The temperature and wax profiles in turbulent flow are found by solving the energy and mass balance equations which are now modified to represent the turbulent velocity and the diffusion rate under turbulence. The energy and mass balance equations are (Lee, 2008)

Mass Transfer $$v_z \frac{\partial C}{\partial z} = \frac{1}{r}\frac{\partial}{\partial r}\left[r(\varepsilon_M + D_{wo})\frac{\partial C}{\partial r}\right] - k_r(C - C_{ws}) \ \ and \tag{66}$$

Heat Transfer $$v_z \frac{\partial T}{\partial z} = \frac{1}{r}\frac{\partial}{\partial r}\left[r(\varepsilon_H + a_T)\frac{\partial T}{\partial r}\right], \tag{67}$$

where, $\frac{\varepsilon_M}{D_{wo}} = \frac{Sc}{Sc_T}\frac{\varepsilon}{\nu}$ , $\frac{\varepsilon_H}{a_T} = \frac{Pr}{Pr_T}\frac{\varepsilon}{\nu}$ , $Sc_T = 0.85 + \frac{0.015}{Sc}$ , $Pr_T = 0.85 + \frac{0.015}{Pr}$ and $v_z = v_z^+\sqrt{\frac{\tau_w}{\rho}}$ in the oil phase and $v_z = 0$ in the deposit.

The momentum eddy diffusivity $\frac{\varepsilon}{\nu}$ is used to calculate the turbulent-diffusivity to non-turbulent diffusivity ratio for both mass and heat diffusivity. It is a function of the dimensionless distance from the oil-wax deposit interface, expressed as $y^+$ (Van Driest, 1956) and the dimensionless turbulent velocity, expressed as $v_z^+$. The formula that gives $\frac{\varepsilon}{\nu}$ is given by the Nikuradse equation (Deen, 1998)

Nikuradse equation $$\frac{\varepsilon}{\nu} = (\kappa y^+)^2\left[1 - exp\left(-\frac{y^+}{A}\right)\right]^2\left|\frac{dv_z^+}{dy^+}\right| \ and \tag{68}$$

$$v_z^+ = \begin{cases} y^+ & y^+ \le 5 \\ 5lny^+ - 3.05 & 5 < y^+ \le 30 \\ 2.5lny^+ + 5.5 & y^+ \ge 30 \end{cases},$$

where $y^+ = \frac{y}{\nu}\sqrt{\frac{\tau_w}{\rho}} = \left(1 - \frac{r}{R}\right)\frac{Re}{2}\sqrt{\frac{f}{8}}$ , $f = \frac{0.305}{Re^{0.25}}$ , κ = 0.4 and A=26 (Deen, 1998).

Equations (66) and (67) are discretized and solved in exactly the same way as the governing equations for laminar flow (equations (53) and (54)). The only differences being in the velocity calculation and in the diffusivity calculation on which now the turbulence term is added.

### 3.11.5. The Precipitation Rate Constant $k_r$.

The precipitation rate constant $k_r$ expresses the growth rate of wax nucleus in supersaturated solution. If the solution is not supersaturated, or equivalently the temperature is above the WAT, then $k_r$ is zero. In this case, the wax deposition rate can be accurately calculated by the IHMT model (section 3.9). For an increased $k_r$ that approaches to infinity *the wax concentration becomes close to the thermodynamic equilibrium concentration, $C_{ws}(T)$, which represents the lower-bound solubility model* (Z.Huang, 2011).

As per Lee (Lee, 2008), $k_r$ can be expressed by combining the correlation for diffusivity given by Hayduk and Minhas (Hayduk, 1982), given in equation(17) with the Arrhenius equation for the viscosity:

Arrhenius equation

$$\mu = \mu_{cloud}\, exp\left[\frac{E}{R}\left(\frac{1}{T} + \frac{1}{T_{cloud}}\right)\right] \quad and \tag{69}$$

$k_r$ as a function of $k_{r,cloud}$

$$\frac{k_r}{k_{r,cloud}} = \left(\frac{T}{T_{cloud}}\right)^{1.47} exp\left[\frac{\gamma E}{R}\left(\frac{1}{T} - \frac{1}{T_{cloud}}\right)\right], \tag{70}$$

where, $E$ (J/mol) is the activation energy and R the ideal gas constant (8.314 J/K/mol).

## 3.12. Wax Deposit Growth and Aging.

The wax deposit is described by its thickness and its content in wax. The wax precipitates not only at the surface of the deposit but also in cavities existing within it. The more these cavities are filled the more wax precipitates at the surface, increasing the deposit's thickness.

### 3.12.1. Aging of the Wax Deposit.

The wax deposit is changing with both in thickness and constitution. The change in constitution is accredited to the diffusion of wax towards the deposit and oil diffusing out of it. This phenomenon is known as aging. In equation form it is written as:

(P.Singh, 2001)

Rate of change of wax in the deposit = Radial convective flux of wax molecules from the bulk to the fluid-gel interface

$$\frac{d}{dt}\left[\pi\left(R^2 - r_i^2\right)\bar{F}_w(t)L\rho_{gel}\right] = 2\pi r_i L k_M [C_{wb} - C_{ws}(T_i)]\,. \tag{71}$$

According to Singh et al. (P.Singh, 2000), the gel density $\rho_{gel}$ is constant and does not vary with time because the densities of the oil and the wax are equal. Hence the growth equation is written as:

$$\pi\left(R^2 - r_i^2\right)\frac{d\bar{F}_w(t)}{dt} - 2\pi r_i \bar{F}_w(t)\frac{dr_i}{dt} = \frac{2\pi r_i k_M}{\rho_{gel}}[C_{wb} - C_{ws}(T_i)] \tag{72}$$

The above equation can be transformed in a way that $r_i$ is replaced by the dimensionless thickness $y$. The transformation is $y=1-r_i/R$ and its application yields the expression for aging

Aging equation

$$\frac{y}{1-y}\left(1 - \frac{y}{2}\right)\frac{d\bar{F}_w(t)}{dt} + \bar{F}_w(t)\frac{dy}{dt} = \frac{k_M}{\rho_{gel}R}[C_{wb} - C_{ws}(T_i)]\,. \tag{73}$$

### 3.12.2. Growth of the Wax Deposit.

The deposit growth is related to the mass transfer equations (53) and (66). The amount of wax not carried away by convection is diffused towards the wall and deposits, excluding the amount of wax that precipitates on its way towards the deposit. The next stage is at the interface, were the wax molecules enter the deposit but not necessarily deposit directly. They may still remain in solution with the oil trapped within the deposit. So, the amount of mass deposited is divided in the wax coming from the bulk oil and the wax coming from the trapped oil. These are separated because the diffusion rate of the wax within them differs and so they contribute in the deposit growth with

| | | | | | |
|---|---|---|---|---|---|
| Rate of addition of wax in growing the gel deposit | = | Radial convective flux of wax molecules from the bulk to the fluid-gel interface. | - | Diffusive flux into the gel at the gel interface. | (74) |

different rates. The total growth rate is the sum of the two and is expressed as (P.Singh, 2000)

In terms of *y*:

Growth equation

$$\bar{F}_w(t)\rho_{gel}\frac{dy}{dt} = \frac{k_M}{R}[C_{wb} - C_{ws}(T_i)] + \frac{D_e}{R}\frac{dC_{ws}}{dT}\frac{dT}{dr}\Big|_i. \quad (75)$$

NOTE: In the Aging and Growth equations the mass transfer coefficient $k_1$ as proposed by Singh et al., has been replaced by $k_M$ , as proposed by Lee and Huang (Z.Huang, 2011) (Lee, 2008). See section 2.2.

## 3.13. Thermal Conductivity of the Pipe-Wall and the Gel Deposit.

### 3.13.1. Thermal Conductivity of the Pipe-Wall Layers

The design of pipes used in subsea oil extraction must deal with multiple problems. The ideal pipe should be reelable for easier installation and avoidance of discontinuities across the pipeline, it should be resistant to galvanic corrosion and it should withstand any hydrostatic or other stresses. Additionally, the pipe must thermally insulate the crude oil within from the surrounding sea water sufficiently. There is a maximum limit to the amount of insulation as it reduces the specific weight of the pipeline and makes it buoyant. In this study, a typical pipe section is used (Bai) which is shown in Figure 7.

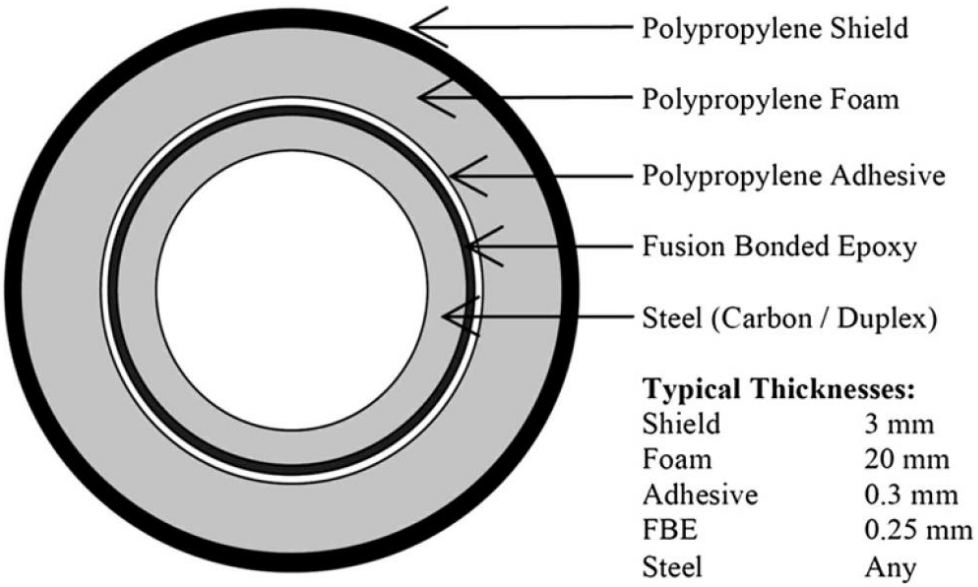


**Figure 16:** Pipe cross section. **(Bai)**

Each layer has its own heat transfer coefficient indicative of which is the U-value (W/m2K). Table 1 lists heat insulating materials with maximum applicable depth and corresponding U-values (Bai).

Under pressure, as is the case in deep waters, the materials in the outer layers of the pipe compress and their U-value changes. For this study, the outer layer is considered to be a combination of materials with U-value equal to 0.2 W/m2K. Material aging is another cause for reduced heat

insulating capability, also referred to as creep. In this study, the time frame is a few weeks which is too short for the creep to be taken into account.

**Table 2:** Pipe Insulating Materials **(Bai)**

| Name of Coating System | Max. Depth (m) | Conductivity ($W/m^2K$) |
|---|---|---|
| Polypropylene-solid | 3000 | 0.22 |
| Polypropylene-reinforced foam combination | 600 - 3000 | 0.13 – 0.22 |
| Polyurethane-glass syntactic | 2000 - 3000 | 0.12 – 0.17 |
| Epoxy syntactic | 2000 – 3000 | 0.10 – 0.135 |

Additional insulation delays the loss of temperature and in turn the deposition of waxes. In the case of thicker insulation, the oil bulk is richer in wax when it reaches the peak point resulting in a wider and slightly taller peak (Figure 17). The following plots show the effect of thicker insulation on the wax deposit thickness. The first plot is for insulation layers 24 mm thick, while the other is for insulation layers 48 mm thick.

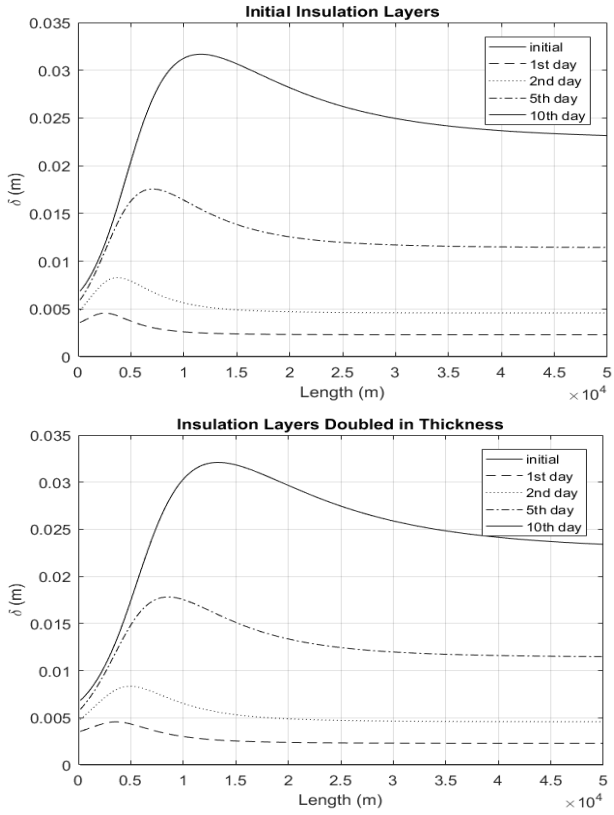


**Figure 17:** Wax deposit thickness along a pipeline.

As the gel deposit ages and the mass fraction of wax increases, the thermal conductivity of the deposit increases. Singh et al. use the following Maxwell correlation (Carslaw, 1959) in their model to find the thermal conductivity of the gel deposit:

$$k_{dep} = \frac{2\,k_{cond}^{wax} + k_{cond}^{oil} + (k_{cond}^{wax} - k_{cond}^{oil})\,\overline{F}_w}{2\,k_{cond}^{wax} + k_{cond}^{oil} - 2\,(k_{cond}^{wax} - k_{cond}^{oil})\,\overline{F}_w}\,k_{cond}^{oil}\,. \tag{76}$$

This is a combination of the oil and the wax conductivity. Note that the paraffin wax is a better heat conducer than oil, thus is has a higher conductivity coefficient. Nonetheless, the overall insulation due to wax deposition increases over time as the wax deposit thickens.

## 3.14. Variation of Dynamic Viscosity as a Function of Temperature.

As with all substances, the crude oil dynamic viscosity increases with the drop of temperature. For some oils, when the temperature drops below the cloud point, their viscosity greatly increases and even solidify. These types of oils are out of the scope of this study. Instead, the oil samples analyzed here have a subzero cloud point. Even below that their viscosity reaches a maximum that does not prohibit flow. The oil samples used are the Oil 1 and Oil 2 from the paper 'Wax Precipitation from North Sea Crude Oils. 1.Crystallization and Dissolution Temperatures, and Newtonian and Non-Newtonian Flow Properties' (H.P.Ranningsen, 1991). From these data, two polynomial expressions of the dynamic viscosity were formed (Figure 18).

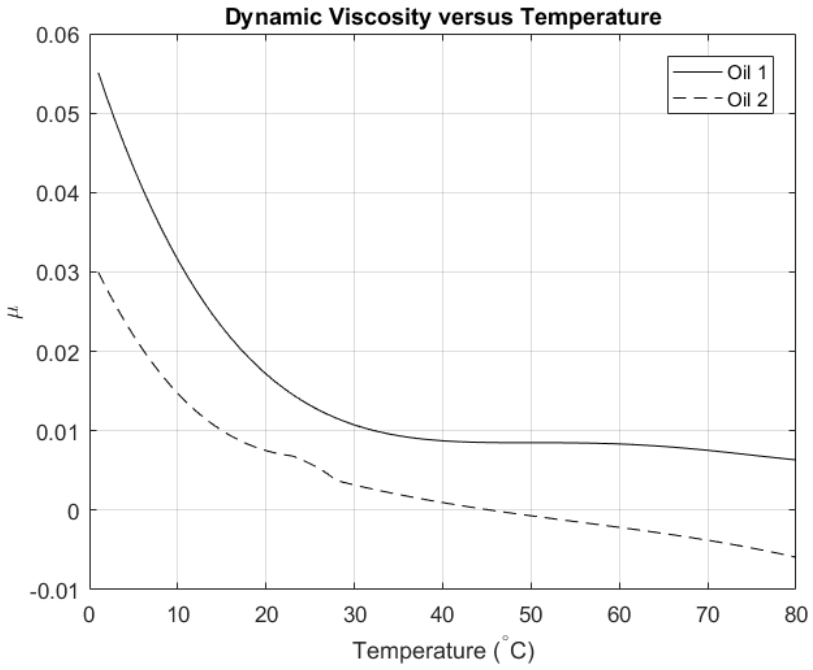


**Figure 18:** Dynamic Viscosity for Oil 1 and Oil 2

The expression for the dynamic viscosity for Oil 2 consists of two different polynomial functions. One for a low temperature range and one for a high for better accuracy. This creates a discontinuity which is dealt with a convex combination of the two expressions.

# Chapter 4: Application of the Wax Deposition Model on a Segmented Subsea Pipeline.

The properties of the crude oil change as its pressure and temperature drop along the pipeline. The wax deposition models are validated for steady state conditions. To approach these conditions the pipeline is segmented in many parts of relatively small length on each of which the conditions are virtually steady. That allows the application of the wax deposition models.

## 4.1. Viscous Losses Calculation for Changing Parameters Along a Segmented Pipeline.

The flow rate affects the wax deposition mainly due to the amount of mass carried through the pipeline. Parameters like the Nu and Re numbers vary as well, but the wax deposition rate is not as sensitive on those as on the flow rate. The flow rate calculation involves the resistances along the pipeline and the pressure drop along its length. In this study, the pressure at the entrance of the pipeline and at the exit are considered steady and so is the total pressure drop. The formula is

$$Q = \frac{\Delta P}{R}, \tag{77}$$

where Q is the flow rate in $m^3/s$, ΔP is the pressure drop in Pa and R is the resistance in Pa s $/m^3$.

For a segmented pipeline model, the resistance is the sum of the resistances of each segment. The resistance in turn, is a function of the flow rate

$$R = f_{tp}\left(\frac{8L\rho_{eq}Q}{\pi^2 D^5}\right), \tag{78}$$

where f is the friction factor given equation (43)

Equation (77) is solved numerically with the bisection method for Q. On each iteration the temperature distribution and dynamic viscosity are calculated. The dynamic viscosity of the crude oil changes with temperature and the relations used in this study are given for Oil 1 and Oil 2 (H.P.Ranningsen, 1991).

Regarding a long pipeline, the temperature drops along its length, which in turn increases the fluid's viscosity and in turn the viscous losses. Another parameter that changes in a non-linear fashion is the pressure as the viscous losses are not the same on every given point of the pipeline. To include all these in the viscous losses calculation, the pipeline must be separated in segments of relatively short length, within which the flow and temperature do not change significantly. To accurately calculate both the viscous losses and the flow, equation (77) is solved with the bisection method and inside each iteration the flow is determined for each segment. The solution algorithm is as follows:

**INITIALIZATION**
Set the range for Q = [$Q_{min}$ ,$Q_{max}$].
**SOLUTION LOOP**
While $abs(\frac{abs(P(1)-P(end)}{\Delta Ptotal} - 1) >$ error
*R = 0* (Total Resistance – Viscous Losses)
For: 1st segment to last Calculate:
Run the Beggs and Brill model
$Re_{two\_phase}$ (50)
Equivalent dynamic viscosity $\mu_{eq}$.
Equivalent density $\rho_{eq}$.
$\Delta P_f$ (44)
Viscous losses R of the segment (78) (*R_segment*)
*R =R+R_segment;*
Pressure drop and pressure calculation for the next segment.
Oil average speed $v_{oil} = Q/A_{flow}$
Temperature distribution from equation (26) section 3.8.1
Dynamic viscosity $\mu$ (used to find $\mu_{eq}$ in the next segment).
End
Find $(\frac{abs(P(1)-P(end)}{\Delta Ptotal} - 1)$

If $\frac{abs(P(1)-P(end)}{\Delta Ptotal} - 1 > 0$ (Q is not high enough)
$Q_{min}$ = Q
Elseif $\frac{abs(P(1)-P(end)}{\Delta Ptotal} - 1 \leq 0$ (Q is not higher than allowed by the losses)
$Q_{max}$ = Q
End
Find $Q = \frac{Q_{max}+Q_{min}}{2}$
End
Recalculate the Beggs and Brill for the last value of *Q*.

Once the flow has been determined throughout the pipeline for each segment, the Combined Heat Mass Transfer model may be applied.

## 4.2. Computation of the Gel Deposit Aging and Growth Equations.

Following the algorithm used by Singh et al. in their relevant study (P.Singh, 2000) the aging and growth of the gel deposit are solved for each time step using the 4$^{th}$ order Runge-Kutta method. In the Singh et al. study the computational time-steps were initially *30 sec* till *time = 10 min*, then, as the wax deposition rate declines the time-steps increased to *2 min* till *time = 1 h* and finally they increased to *10 min. That numerical scheme was tested for convergence and stability and found to be robust* (P.Singh, 2000). In this study, where the pipe discretization is higher, the time steps are set at *10 sec*.

The first Runge-Kutta step (R-K step) begins for the given time point from the first segment. The initial wax concentration profile and temperature coming out of the well are used to initialize the combined heat-mass transfer calculation. The appropriate heat-mass transfer model is used whether the flow is laminar or turbulent in the segment. The wax concentration and temperature profiles at the end of the segment are used to initialize the heat-mass transfer solution of the next segment, where the flow might differ. Once all the pipeline has been swept, the slope of the dimensionless thickness *y* and the wax mass fraction in the deposit $\bar{F}_w$ have been calculated at the given time.

There are two functions equal to the first derivatives of $\bar{F}_w$ and *y* respectively, based on which the Runge Kutta coefficients $K_1$, $K_2$, $K_3$, $K_4$ are calculated

$$\frac{dy}{dt} = \frac{\frac{k_1}{R}[C_{wb} - C_{ws}(T_i)] + \frac{D_e dC_{ws} dT}{R \quad dT \quad dr}\Big|_i}{\bar{F}_w(t)\rho_{gel}} \quad and \tag{79}$$

$$\frac{d\bar{F}_w(t)}{dt} = \frac{\frac{k_1}{\rho_{gel} R}[C_{wb} - C_{ws}(T_i)] - \bar{F}_w(t)\frac{dy}{dt}}{\frac{y}{1-y}\left(1 - \frac{y}{2}\right)}. \tag{80}$$

Let *P* be the array of parameters re-calculated for each R-K step:

$$P = \left[k_1, \left.\frac{dT}{dr}\right|_i, C_{wb}, C_{ws}, \frac{dC_{ws}}{dT}, D_e\right]. \tag{81}$$

Note that the flow on each segment does not change throughout the R-K steps. Thus, any change in the parameters of the *P* array are due to the change in the dimensionless thickness *y* and the wax mass fraction in the deposit $\bar{F}_w$.

In the ensuing R-K steps the *y* and $\bar{F}_w$ are calculated using the slope and their respective values in the previous time step and in turn the *P* array is re-calculated using the new vales of *y* and $\bar{F}_w$.

The R-K algorithm for a time step from point *t* to *t+1* is:

| Step | R-K calculation |
|---|---|
| R-K 1 | $\left.\begin{matrix} y_i \\ \bar{F}_{w_i} \\ P_i \end{matrix}\right\}$ *initial values*<br>Solve the Combined Heat-Mass Transfer Model<br>$K_{1y} = \frac{dy}{dt}(t_i, \bar{F}_{w_i}, y_i, P_i)$<br>$K_{1Fw} = \frac{d\bar{F}_w}{dt}(t_i, \bar{F}_{w_i}, y_i, P_i, K_{1y})$ |
| R-K 2 | $y_{i2} = y_i + \frac{K_{1y}}{2}dt$<br>$\bar{F}_{w_{i2}} = \bar{F}_{w_i} + \frac{K_{1Fw}}{2}dt$<br>$P_{i2}$ *= parameter values recalculated for* $y_{i2}$ *and* $\bar{F}_{w_{i2}}$<br>Solve the Combined Heat-Mass Transfer Model<br>$K_{2y} = \frac{dy}{dt}(t_i + \frac{dt}{2}, \bar{F}_{w_{i2}}, y_{i2}, P_{i2})$<br>$K_{2Fw} = \frac{d\bar{F}_w}{dt}(t_i + \frac{dt}{2}, \bar{F}_{w_{i2}}, y_{i2}, P_{i2}, K_{2y})$ |
| R-K 3 | $y_{i3} = y_i + \frac{K_{2y}}{2}dt$<br>$\bar{F}_{w_{i3}} = \bar{F}_{w_i} + \frac{K_{2Fw}}{2}dt$<br>$P_{i3}$ *= parameter values recalculated for* $y_{i3}$ *and* $\bar{F}_{w_{i3}}$<br>Solve the Combined Heat-Mass Transfer Model<br>$K_{3y} = \frac{dy}{dt}(t_i + \frac{dt}{2}, \bar{F}_{w_{i3}}, y_{i3}, P_{i3})$ |

| | |
|---|---|
| | $K_{3Fw} = \frac{d\bar{F}_w}{dt}(t_i + \frac{dt}{2}, \bar{F}_{w\,i3}, y_{i3}, P_{i3}, K_{3y})$ |
| R-K 4 | $y_{i4} = y_i + \frac{K_{3y}}{2}dt$<br>$\bar{F}_{w\,i4} = \bar{F}_{w_i} + \frac{K_{3Fw}}{2}dt$<br>*$P_{i4}$ = parameter values recalculated for $y_{i4}$ and $\bar{F}_{w\,i4}$*<br>Solve the Combined Heat-Mass Transfer Model<br>$K_{4y} = \frac{dy}{dt}(t_i + dt, \bar{F}_{w\,i4}, y_{i4}, P_{i4})$<br>$K_{4Fw} = \frac{d\bar{F}_w}{dt}(t_i + dt, \bar{F}_{w\,i4}, y_{i4}, P_{i4}, K_{4y})$ |
| *Step i+1* | $y_{i+1} = y_i + \frac{1}{6}(K_{1y} + 2K_{2y} + 2K_{3y} + K_{3y})dt$<br>$\bar{F}_{w\,i+1} = \bar{F}_{w_i} + \frac{1}{6}(K_{1Fw} + 2K_{2Fw} + 2K_{3Fw} + K_{4Fw})dt$ |

## 4.3. Computational Flow Chart.

FOR EACH TIME STEP THE SYSTEM IS CONSIDERED TO BE IN STEADY

START BY FINDING THE FLOW RATE ITERATIVELY.
GIVEN: Pin, Pout, Tin, Tambient, Oil properties, Pipe dimensions and insulation.

INITIALIZE Q
WHILE $Q_{i+1}$-$Q_i$ > error
FOR EACH SEGMENT OF THE PIPELINE

Beggs and Brill Correlation: Equivalent viscosity, density. Two phase Re and friction factor f.

Calculate Resistance of the Segment and Pressure Drop.

Temperature distribution.

Calculation of base Viscosity as a function of the segment's average temperature.

END
SUMMATE RESISTANCES
CALCULATE $Q_{i+1}$
CALCULATE $Q_{i+1}$-$Q_i$
END

OUTPUTS: T distribution, Flow rate, equivalent viscosity/density for each segment.

WAX DEPOSITION MODEL: On each segment find the amount of wax deposited starting from the entrance of the pipe. The wax deposited is subtracted from the wax available in the next segment. For each segment the wax deposition is calculated with the following 4$^{th}$ order Runge-Kutta algorithm:

RUN the wax deposition model for time step i. GIVEN:
dT/dr, $k_1$, $C_{wb}$, $C_{ws}$, $dC_{ws}/Dt$ @ the interface, De, ID, $F_w$

ASSUMING THAT THE FLOW DOES NOT CHANGE!
FOR i=1:4
FIND for time i*dt/4: dT/dr, $k_M$, $C_{wb}$, $C_{ws}$, $dC_{ws}/Dt$ @ the interface, De, ID, $F_w$,.
RUN the wax deposition model for the appropriate time step using as inputs the outputs of the previous time step where applicable.

## Chapter 5: Results and Discussion

In this section, two cases are run, one for each of the available oil samples.

### 5.1. Code Validation of the Wax Deposition Model

The Singh-et-al problem, which is a one-dimensional problem, was validated using data from the respective publication (P.Singh, 2000). As developed in section 3.3 the experiment was conducted inside flow loop with a stirred tank and a pump. The oil temperature is increased inside the tank and so there is no precipitated wax in the bulk of the oil. The use of the pump forces the fluid around the loop at a certain flow rate and so the viscous losses calculation is not needed. Finally, the oil used is the Food Grade Wax 'Mobil M140', a fabricated mix of kerosene with standard concentrations of heavy carbon-chains.

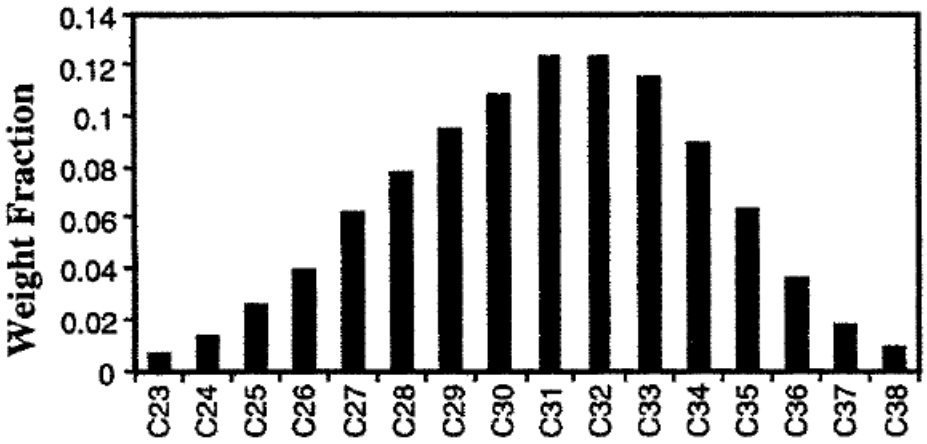


**Figure 19:** Weight fraction distribution of components in the M140 oil. **(P.Singh, 2000)**.

The oil viscosity can be calculated from the weight fraction distribution by the linear combination of each component's viscosity multiplied by the respective fraction weight. The oil viscosity at room temperature is 8.7 mPa·s and the density is 838.5 kg/m$^3$.

The solubility curve is the same as given by equation (20) and it's plot is shown on Figure 20. As in the conducted experiment, the entry temperature of the oil into the loop is at 22.2°C. The case used to validate the code is the one where the wall temperature is at 4.4°C and the flow rate is at 6.3 $10^{-5}$ $m^3/s$ corresponding to Re=540.

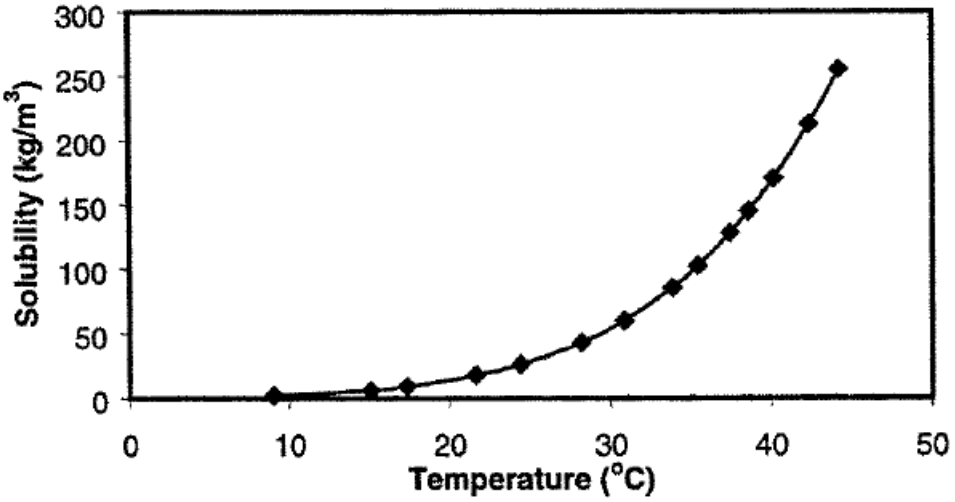


**Figure 20:** Solubility of the M140 oil versus temperature. **(P.Singh, 2000)**.

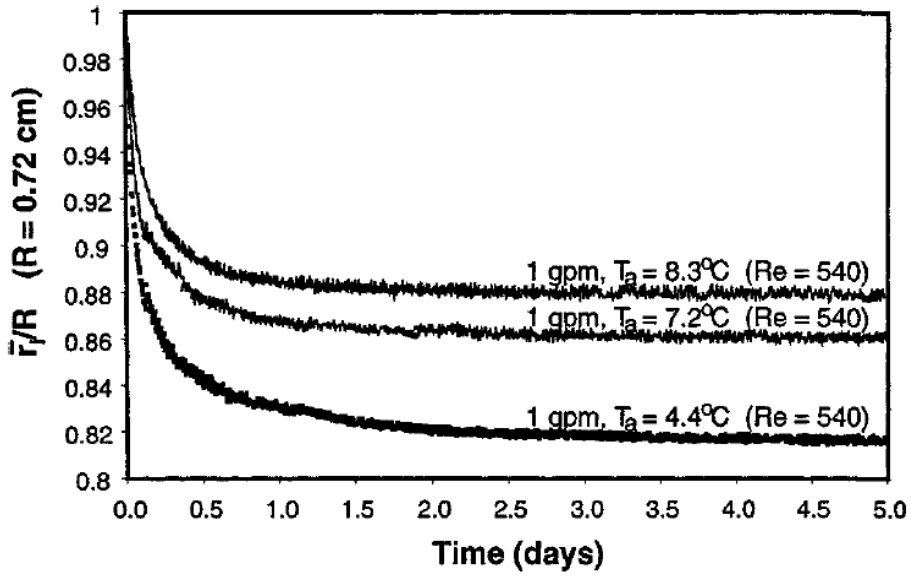


**Figure 21:** Ratio of flow radius r to pipe inner radius R over time. **(P.Singh, 2000)**

The ratio of r/R=0.83 corresponds to wax deposit thickness $\delta$ = 1.2 $10^{-3}$ m. This result is matched by the wax deposition code (Figure 22). To reach this result a grid sensitivity was conducted on the 2.44 m (8 ft.) flow loop which showed that at 450 points are needed to have accurate results. Eventually the code was run for 500 points. As shown in the Singh et al. paper, the wax deposit thickness reaches a maximum which is related to the depletion of the wax content in the oil.

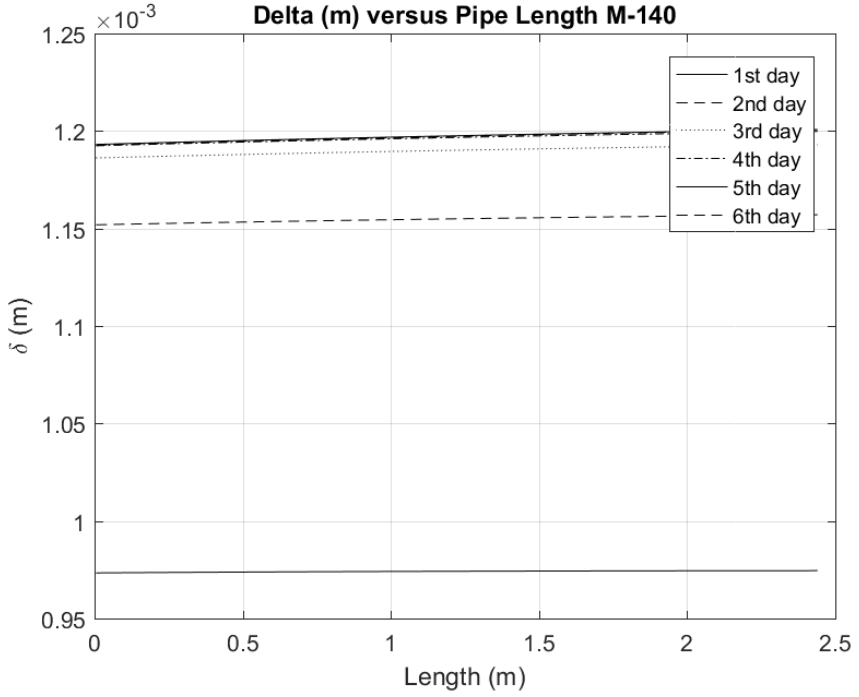


**Figure 22:** Wax deposit thickness versus time.

## 5.2. Variation of the Wax Deposit Thickness for Different GVF on the Flow Loop.

As in the Singh et al. paper, the wax deposition thickness stops increasing after a point due to the reduction of the wax pool in the flow loop. The same holds true for 2-phase simulations but the thickness of the deposit is quite different. In the following figures (Figure 23, Figure 24) the wax deposit thickness is plotted along the flow loop length for various GVF values. Evidently the GVF value has an effect on the distribution of the wax thickness.

It must be noted at this point, that all the wax deposition models depend on 1-phase correlations and on diffusion rates for 1-phase fluids. Thus, the code does not receive as input a change in the oil mass, but only a change in the *Nu*, *Re* and *Sh* numbers. In order to acquire results that show the effect of the GVF increase, the diffusion rate must be given as a function of GVF.

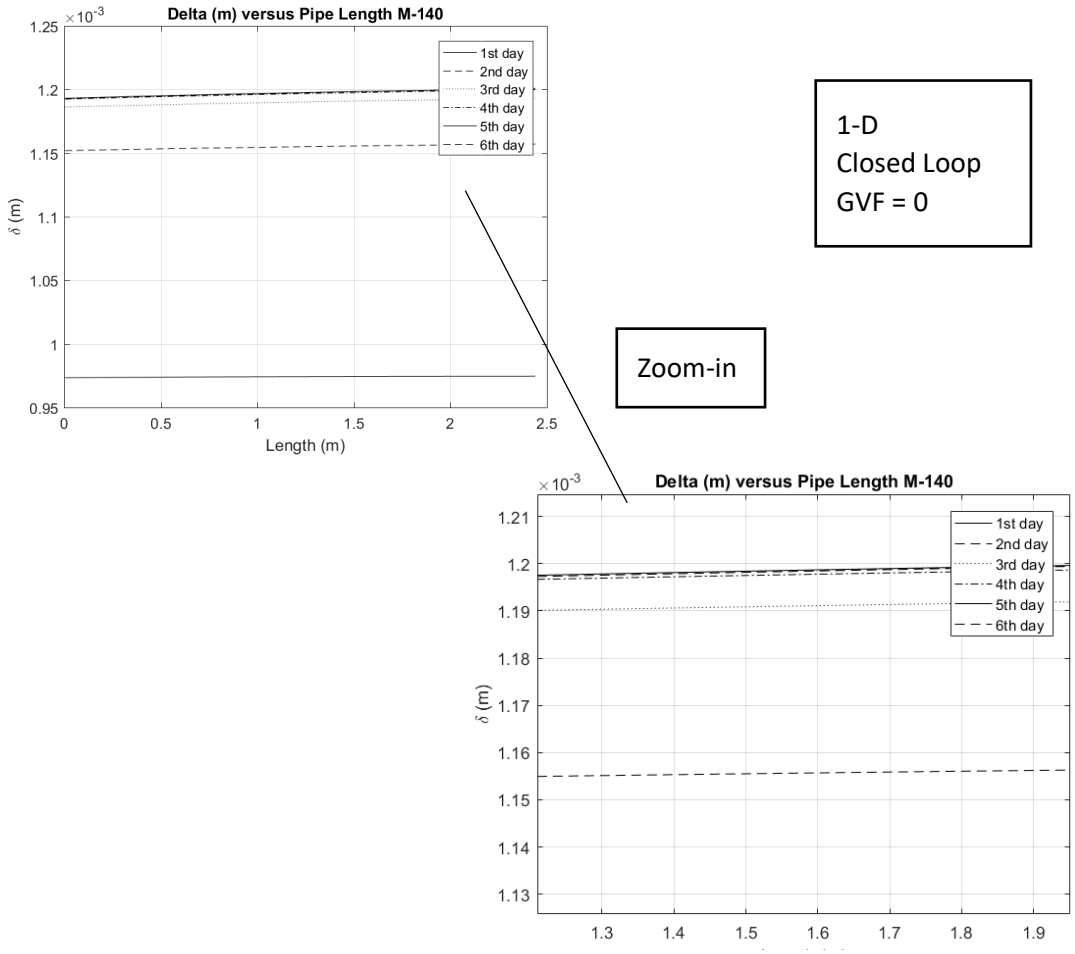


**Figure 23:** Wax deposit thickness along the experimental flow loop for 1-phase fluid.

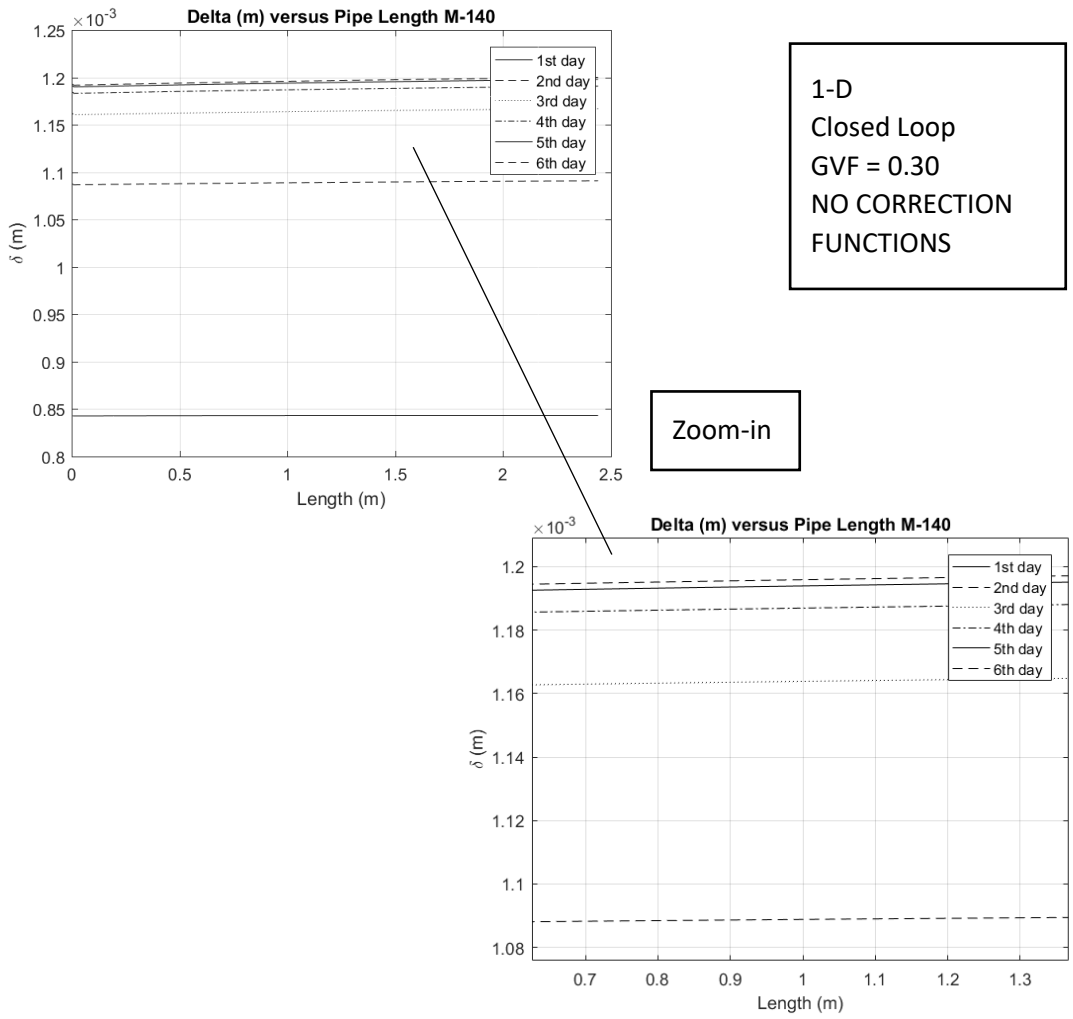


**Figure 24:** Wax deposit thickness along the experimental flow loop for GVF = 0.30.

From what is shown on these simulations, the wax deposit thickness is almost the same for less mass flow rate (same volume flow rate). This calculation paradox is related to the inputs of the wax deposition models, as stated above, which are the *Re*, *Nu* and *Sh* values. So, the 1-phase wax deposition models cannot be applied in combination with a 2-phase fluid model without changing them.

## 5.3. Results After the Addition of a Precipitation Correction Coefficient

Within the targets of this thesis is to provide a model of the wax deposition phenomenon. A complete model should have a correction function on the precipitation rate when applying the 1-phase wax deposition models on top of a 2-phase flow. This should be some function of GVF extracted from experimental results, but for the needs of this thesis's purpose a dummy coefficient is created. That is

$$C_{GVF} = 1 - GVF\ . \tag{82}$$

Then, the aging and growth equations change as follows:

Growth equation
$$\bar{F}_w(t)\rho_{gel}\frac{dy}{dt} = C_{GVF}\frac{k_M}{R}[C_{wb} - C_{ws}(T_i)] + \frac{D_e}{R}\frac{dC_{ws}}{dT}\frac{dT}{dr}\Big|_i \ and \tag{83}$$

Aging equation
$$\frac{y}{1-y}\left(1-\frac{y}{2}\right)\frac{d\bar{F}_w(t)}{dt} + \bar{F}_w(t)\frac{dy}{dt} = C_{GVF}\frac{k_M}{\rho_{gel}R}[C_{wb} - C_{ws}(T_i)]\ . \tag{84}$$

### 5.3.1. Diffusivity Versus Temperature in 1-D Closed Loop

The wax deposition rate relies heavily on the diffusivity. Which in turn is a strong function of temperature. It is worth displaying the diffusivity over time along with temperature and how it changes for different GVF values. The following results are from the emulation of a closed loop with 1-D, 2-phase flow.

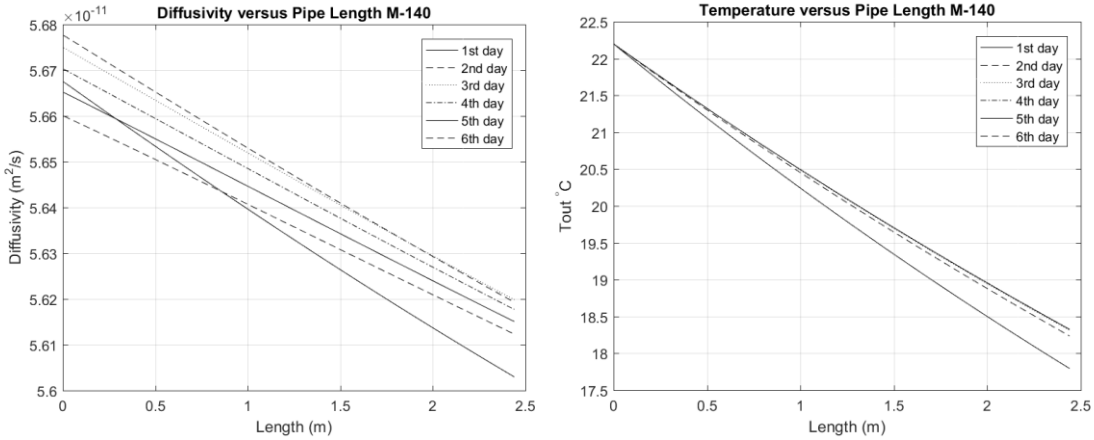


**Figure 25:** Diffusivity and Temperature for GVF = 0.

As per equation (17) the diffusivity depends on the viscosity. Introducing the equivalent viscosity gives a different estimation of the diffusivity. In fact, diffusivity is conversely proportional to viscosity - $\gamma$ in equation (17) is a negative number. So, for smaller viscosity, thus thinner fluid, the diffusivity is expected to decrease. This is confirmed for the case where the gas volume fraction is 0.30. As per Figure 25, Figure 26 and Figure 27 the diffusivity for GVF = 0 is higher than the diffusivity for GVF=0.30. In all cases the diffusivity follows the temperature drop with the same pattern.

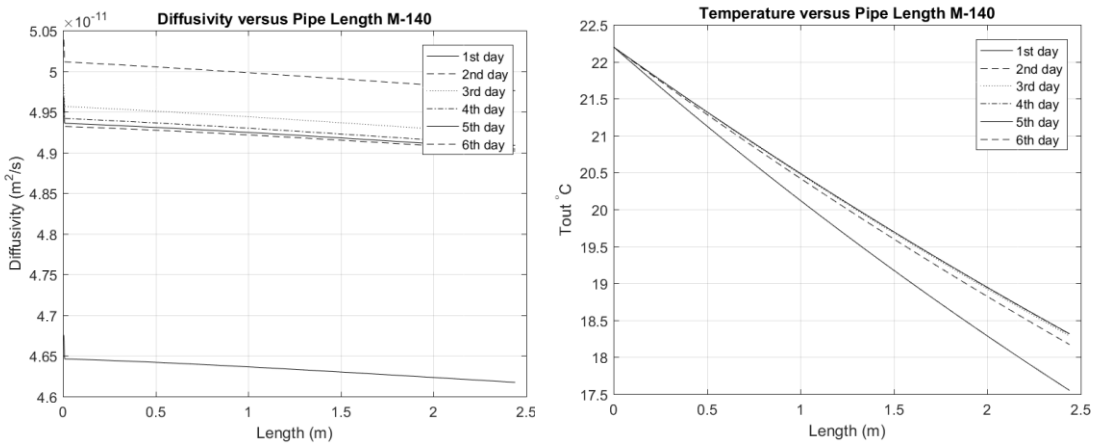


**Figure 26:** Diffusivity and Temperature for GVF = 0.15.

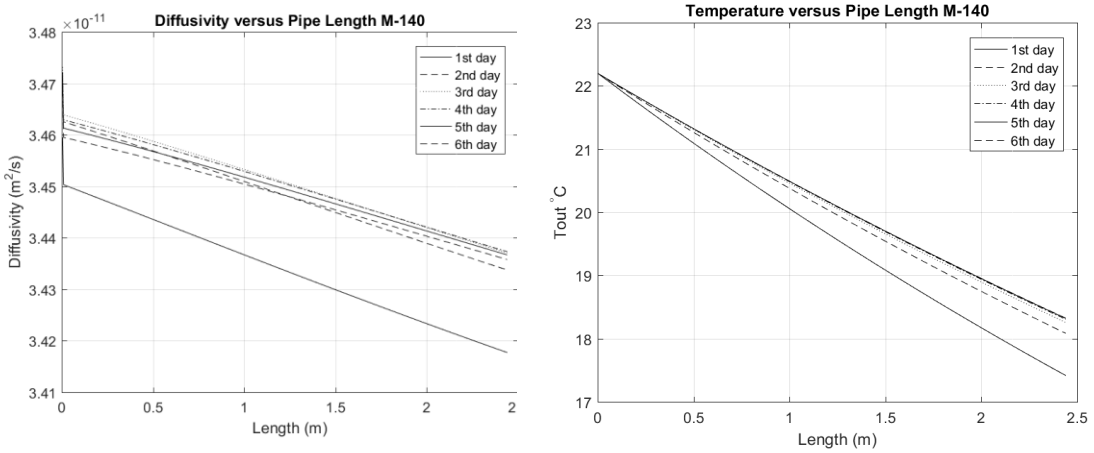


**Figure 27:** Diffusivity and Temperature for GVF = 0.30.

### 5.3.2. Wax Deposition Thickness for Various GVF values in 1-D Closed Loop

In this section the wax deposition thickness is examined, which is the natural result of the diffusivity discussed in the previous section. It is expected that the variations in the wax deposit thickness are proportional to the variations in the diffusivity when the GVF changes, since the wax deposition thickness is proportional to the diffusivity. Note that the 1-D model is the Singh et al. model where the wax precipitated to the wall is overestimated and thus there should be a strong proportionality between the diffusivity and the wax deposit thickness. Also, note that for a more integral model the precipitation correction coefficient $C_{GVF}$ (section 5.35.2 ) is applied.

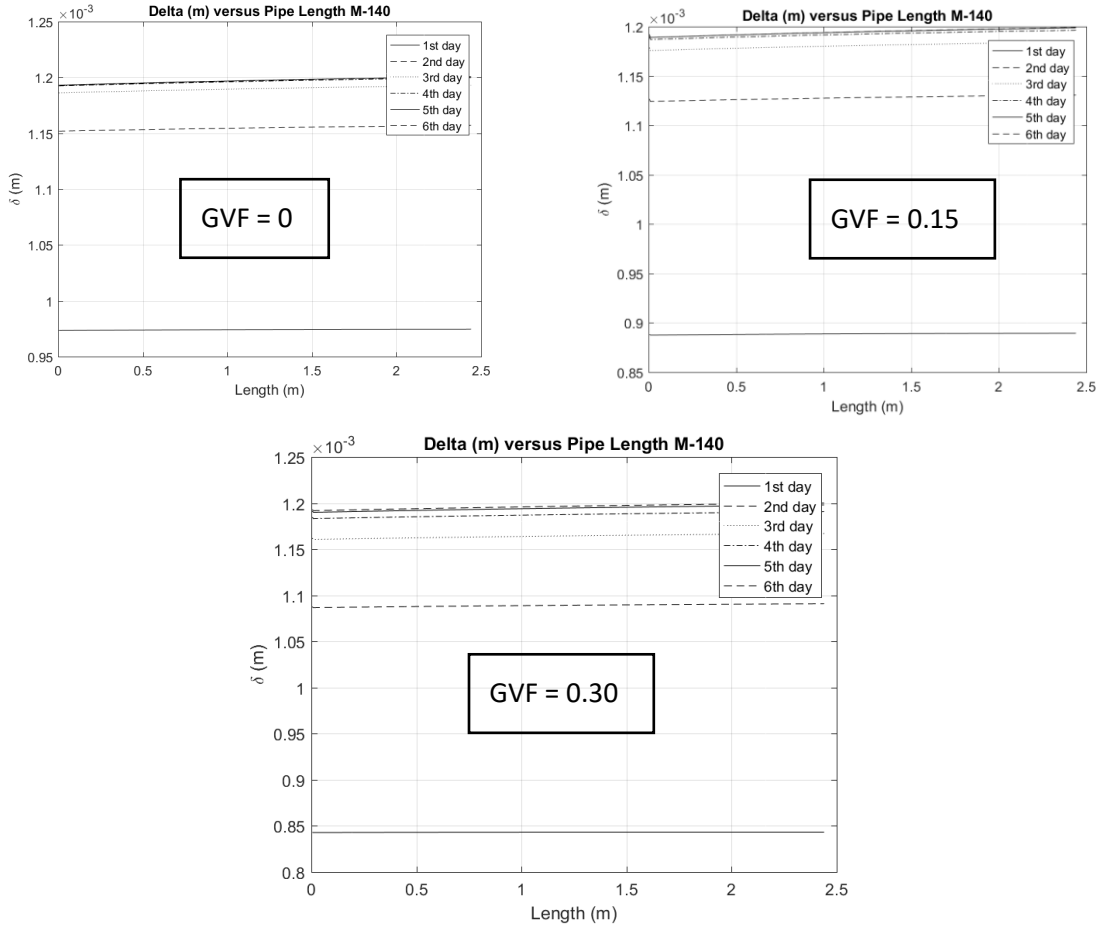


**Figure 28:** Wax Deposition Thickness $\delta$ for various GVF values.

Although the GVF values change, the wax concentration, which is in kg/m$^3$ does not. That means that the oil used in the closed-loop simulation contains the same gross amount of wax and so after

some time it is all precipitated. Thus the final thickness is the same for all cases. The deposition rate though is different. Note that on a real pipeline the wax precipitated in the oil and not at the wall, is not melt in a stirrup tank to be re-circulated in the pipeline as in the closed loop. To draw conclusions from the simulation in this section the wax deposition rate must be examined. Looking at Table 3 at the 2nd day of each case the $\delta$ values are 1.15 mm, 1.13 mm and 1.10 mm for the GVF values 0, 0.15, 0.30 respectively.

The results from this section and the previous (sections 5.3.1and 5.3.2) are shown in the following table:

**Table 3:** Diffusivity and Wax Deposit Thickness Variations

| GVF | Average Diffusivity ($m^2/s\ 10^{-11}$) | % Change in Diffusivity | Average Thickness $\delta$ (mm) | % Change in $\delta$ |
|---|---|---|---|---|
| 0 | 5.64 | | 1.15 | |
| 0.15 | 4.92 | 0.12766 | 1.13 | 0.017391 |
| 0.3 | 3.45 | 0.29878 | 1.1 | 0.043478 |

The change in GVF induced an almost proportional change in the diffusivity. Note once more, that the equivalent viscosity is used in the diffusivity calculation (equation (17)). The same cannot be observed for $\delta$ where the change is very small.

## 5.4. Results of the Simulation Using the Singh et al. Model for Laminar Flow for 1-phase.

The Singh et al model, although it overestimates the wax deposition rate for non-laminar flows, is far less demanding in calculation cost. In this section, two cases are run, one for each of the available oil samples.

**Table 4:** Oil Samples. (H.P.Ranningsen, 1991)

| **Oil Sample** | **Wax Percentage ( wt. kg / kg)** |
|---|---|
| Oil 1 | 2.2 |
| Oil 2 | 6.7 |

The wax deposition rate for Oil 1, that is pourer in wax concentration, is almost twice as low as that for Oil 2. The pipeline is plugged when δ reaches 0.15m.

The oil with higher wax concentration has lower flow rate due to higher amount of wax deposing and reducing the flow section of the pipeline. Oil 1 has higher viscosity despite the lower wax concentration (Figure 18) and consequently its flow rate reduces faster. Also, the flow rate difference does not correspond to the wax deposit difference. It should be bigger for the flow rate since it is a function of the squared flow section radius. Its smaller and the explanation lays on the lower viscosity of the Oil 2. These are shown on Figure 10.

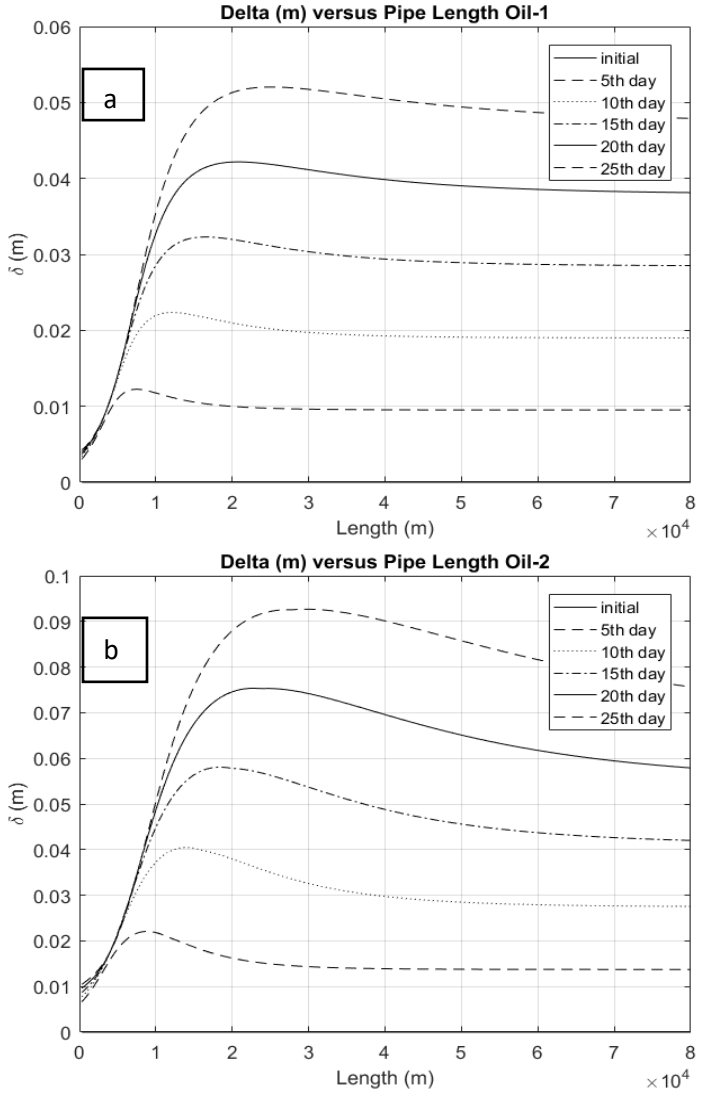


**Figure 29:** Thickness of the wax deposit for 25 days. Plot (a) is for Oil 1 and plot (b) for Oil 2.

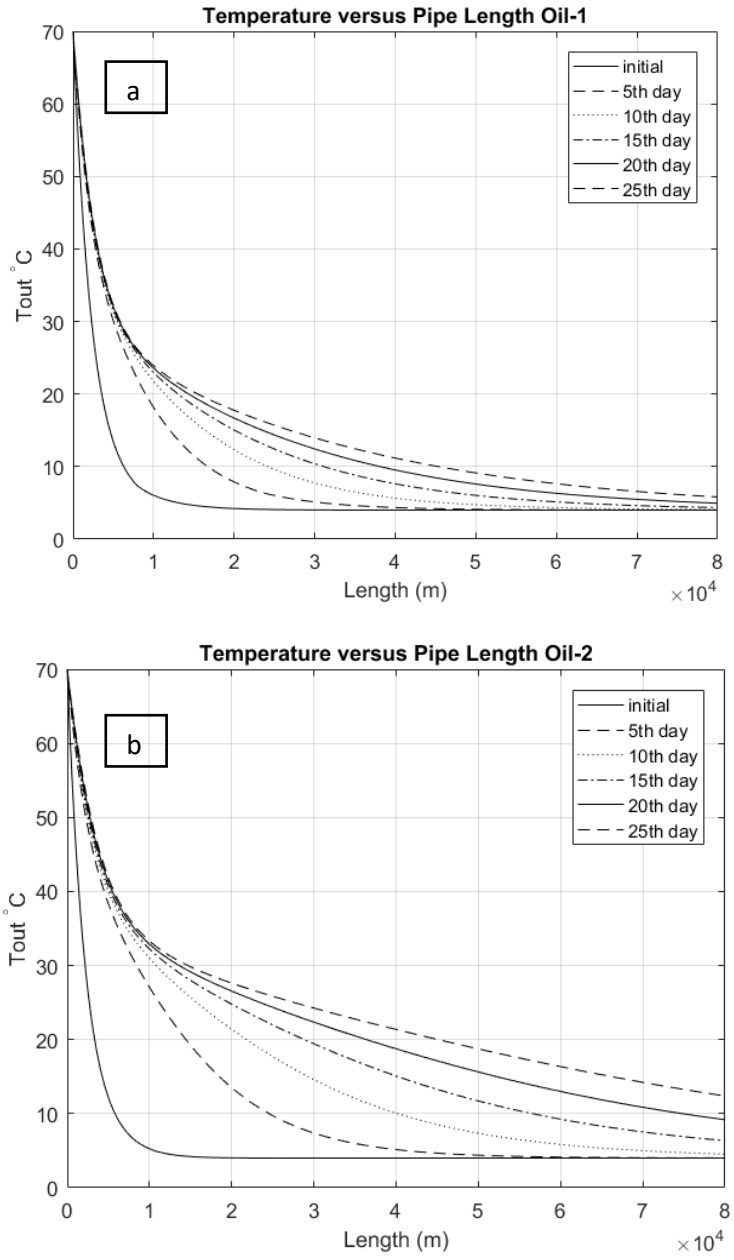


**Figure 30:** Temperature distribution for 25 days. . Plot (a) is for Oil 1 and plot (b) for Oil 2.

The wax deposition thickness is dependent on the temperature distribution through diffusivity and it is expected that the temperature distribution has an effect on the wax deposit thickness. The temperature drop is followed by an increase in the wax deposit thickness. As the wax deposit thickens it adds up to the insulation making the temperature drop less steep (Figure 30). Its effect

on the wax deposit can be seen on Figure 29. The maximum deposition rate is reached later along the pipeline and so the maximum peak of δ shifts to the right as time passes.

The higher the temperature difference between the oil bulk and the external environment the higher the potential that drives diffusion. As time goes by, the wax deposit effectively works as an insulating layer on the pipeline. Consequently, the temperature drop along the pipeline is smaller. Thus result in two things, one is that the oil bulk remains warm enough to keep its wax soluble for bigger pipe lengths. This wax that would otherwise precipitate earlier in the oil bulk increasing its viscosity. The second is that the insulation reduces the temperature potential that drives the diffusion. Note that this potential is the temperature difference between the pipe center and the interior wall. This further reduces the wax deposition rate close to the entrance of the pipeline and allows for more wax deposition further down the pipeline.

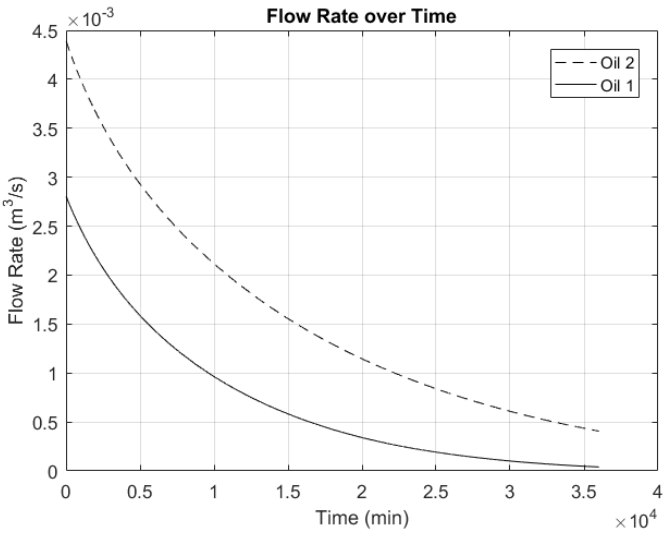


**Figure 31:** Oil flow rates for Oil 1 and Oil 2 in the span of 25 days.

Observing Figure 29, the wax deposit thickness δ is zero at the entrance of the pipeline. As the wax and asphaltene molecules change phase they start diffusing adding up to δ. There is a point where the diffusion reaches a maximum due to temperature difference between the oil bulk and the

sea water. After that the diffusion rate reaches asymptotically a final value and the wax deposition rate remains steady.

As developed in section 16 the Singh et al. model is valid for laminar flow and is slightly inaccurate for transitional flow due to the shear removal (sloughing). For an 80 km pipeline the viscous losses are so high that the fluid does not enter the turbulent regime. Since the Singh et al model is valid, the results of this experiment could be comparable to the real. The flow remains in the laminar region for both oil samples throughout the pipeline for the duration of the experiment as shown on Figure 32.

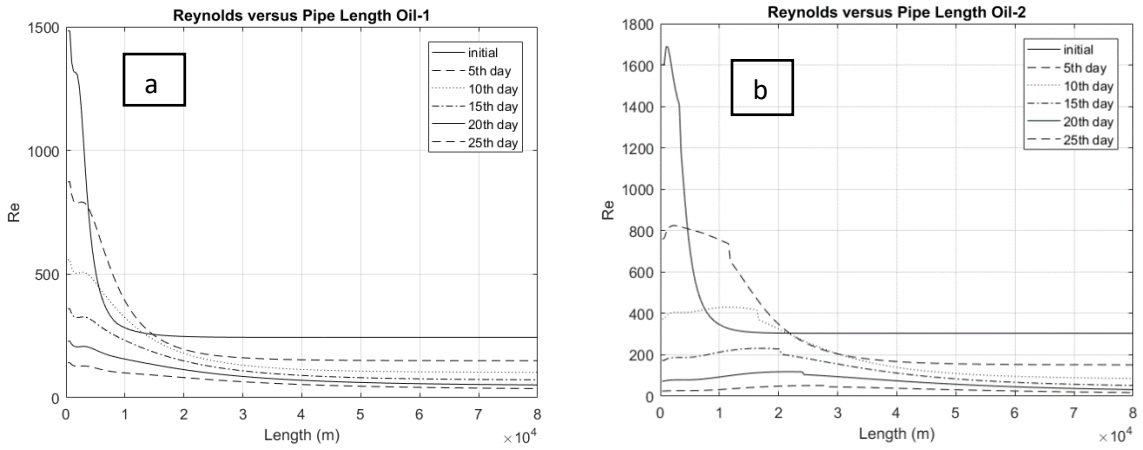


**Figure 32:** Reynolds numbers for (a) Oil-1 and (b) Oil-2 along the pipeline.

## 5.5. Results of the Simulation Using the Independent Heat and Mass Transfer Model

The IHMT model requires the solution of a 2-D flow which adds a lot of calculation cost. Attempting to solve this in parallel in order to save time results in accumulated errors. In the parallel solution the flow is solved serially for the first time step and in consequent steps the flow at the start of each section is that of the previous time step. A main issue with the 2-phase model is that the flow regime may change in a section and that results in high variations in the Re number. The section after the current, where the change occurs, should have an equally high Re variation otherwise discontinuities appear. Indeed, this can be fixed with high discretization, but then running the model in parallel becomes costly and defeats its own purpose.

Failing to reduce the solution time does not allow the application of the IHMT model in long pipelines, typical of the subsea architectures. It does not allow its application for enough simulation time to observe the build-up of wax either.

In this study, the model is applied on a 100m pipe for turbulent flow and on a 1000m pipe for turbulent flow. In the 100m case the length discretization is at 0.1m and in the 1000m case the length discretization is 1m. The discretization sensitivity is different for each case.

### 5.5.1. IHMT Applied on Transitional 2-phase Flow.

As demonstrated in section 5.2 the existing wax deposition models cannot be used for a 2-phase flow. However, this thesis might be the basis for future work where wax deposition models for 2-phase flow will be used. This section demonstrates the current multi-physics model.

A 100m pipe is divided in 10 sections on each of which the flow is solved based on the flow regime of the section. The wax thickness curve is very sensitive in the temperature change which

defines the diffusivity. When the temperature drops below 20 °C the $\delta$ stops growing as fast reaching a plateau at around 5 $10^{-6}$ m (Figure 33).

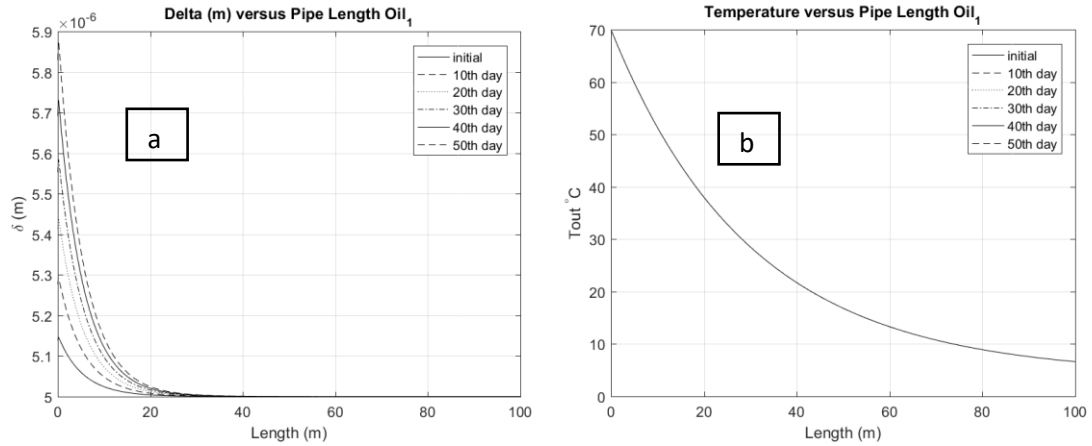


**Figure 33:** Wax deposit thickness (a) and temperature distribution (b) along the pipeline.

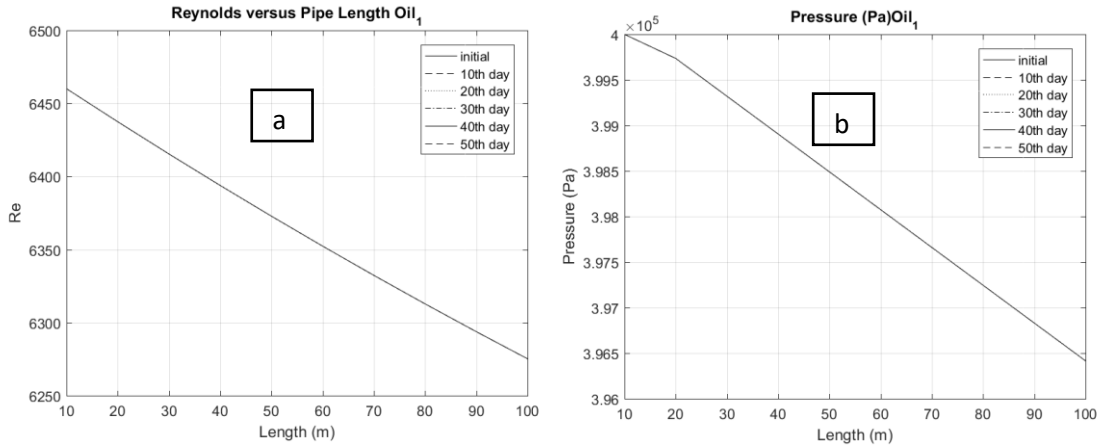


**Figure 34:** Reynolds number (a) and Nusselt number (b) along the pipeline for Oil-1.

The Re number steadily decreases and the pressure drop has the same slope along the pipe except for the entrance part where the deposit thickness is slightly bigger than the rest of the pipeline.

Subsequently a 1000m pipeline is divided in 100 segments and the same solution process is followed as in the 100m pipeline. Again, the wax deposit thickness reaches a plateau as soon as the temperature drops below 20 °C (Figure 35). What changes in a non-linear fashion is the equivalent Reynolds number, which can be explained by a change in the 2-phase flow regime (Figure 36).

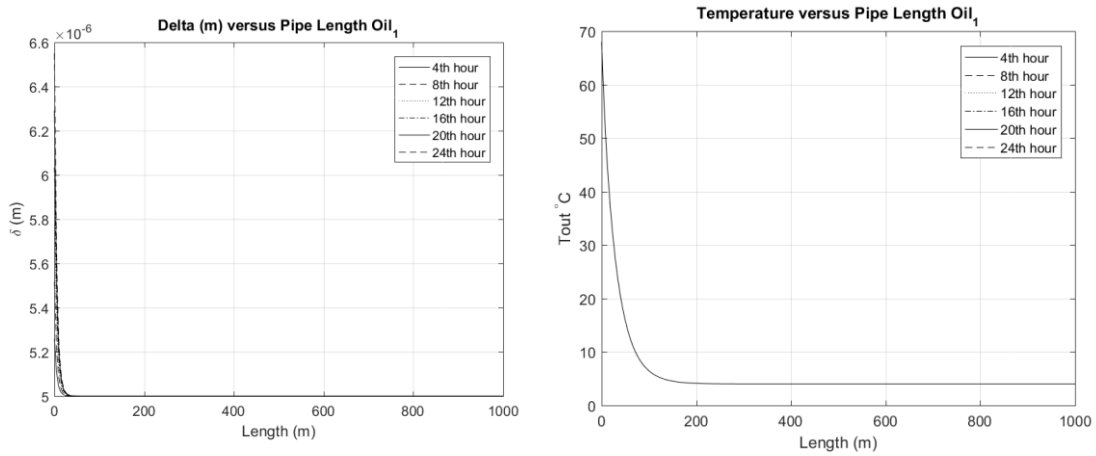


**Figure 35:** Wax deposition thickness along a 1000m pipeline for Oil-1 in 24 hours.

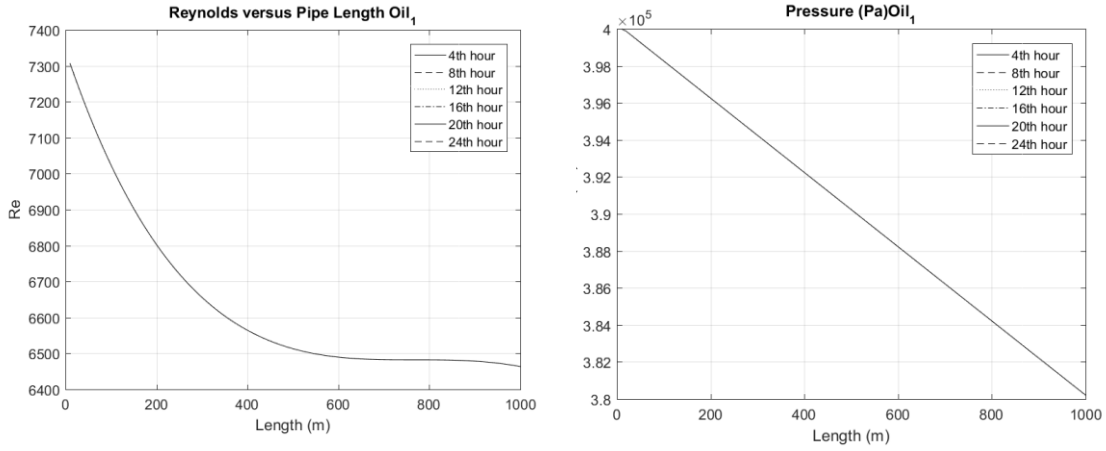


**Figure 36:** Temperature at the center of a 1000m pipeline for Oil-1 in 24 hours.

## 5.6. Summary of Assumptions, Additional to those of the Singh et al. Model and Uncertainty Factors.

The roughness ε of the pipe changes with the deposition of wax. It is expected to increase as a function of the wax deposit thickness. Due to different diffusion rates among the wax components that deposit, the wax crystals formed are expected to be different along the pipeline. Thus the roughness ε is expected to change along the pipe's length. In this study, due to lack of data, the roughness does not change.

The solubility and its derivative versus temperature are a function of temperature and three coefficients (equations (45), (46)). These are unique for each sample, even if the weight concentration in wax is the same between two samples the molecular distribution of C-chains may vary. For this study, the values of a, b, c are the same as those used by Singh et al for their experimental oil-wax mixture.

Similarly, the aspect ratio α affecting the diffusion within the wax deposit (equation (47)) may vary between samples. In this study its considered to be equal to 1.

Also, the pipelines examined here are at the same depth and they are not buried, otherwise there would not be uniformity in the wax deposition.

The viscosity and density are a function of temperature as well as time - pipeline length traveled. As the oil bulk travels along the pipeline its wax concentration is depleted making it less viscous and less dense. For big pipe lengths, were the flow eventually becomes laminar, the flow is not expected to be Newtonian. As the wax diffuses towards the wall, a portion precipitates before reaching the wall. This changes the oil constitution locally whose behavior is expected to be non-Newtonian due to the wax agglomerates. So, the expected flow when not turbulent is expected to be separated to layers with different amounts of precipitated wax. Regarding the density, it changes due to the temperature drop, due to the change in the amount of wax concentration and due to the

phase change of the wax from liquid to solid. These cannot be taken into account due to lack of data.

In addition, the volume balance between the ends of the pipeline is not affected by the amount of wax deposited.

Furthermore, the U-value of the insulating layers is considered to be steady and equal to 0.2 W/m2K.

Finally, the presence of bubbles may have an effect on the amount of wax that precipitated in the oil before reaching the wall. The surface tension on the bubbles may bind the wax molecules which cool down on the bubble surface creating crystallization points. So, the bubbles may increase the amount of wax that precipitates before reaching the wall, decreasing the wax deposition rate and increasing the oil viscosity. It is uncertain which of the two decreases the flow rate the most.

# Chapter 6: Conclusions and Proposal for Future Work.

## 6.1. Conclusions

This thesis attempted to describe the wax deposition phenomenon for subsea pipelines by combining existing fluid, heat transfer and wax deposition models. Starting with 1-phase flow and single dimension simulation of the wax deposition mechanism, the model was built up adding a 2-dimensional simulation combining existing work. The models successfully emulated the results of existing research (section 5.1, (P.Singh, 2000)). Then, the 1-dimensional model was applied for a subsea pipeline, for single phase fluid for a case with laminar flow (section 5.4).

To better approach the actual crude oil flowing in a subsea pipeline, a mechanistic model for 2-phase flow was introduced based on the Beggs and Brill correlation. Since the wax deposit thickness is directly depending on the amount of oil mass passing through the pipe, a better estimation of the 2-phase flow rate should yield more accurate results. The flow rate is accurately calculated. However, when taking the model from the 1-phase flow to the 2-phase flow many uncertainties are introduced. This is because the inputs to the wax deposition model are dimensionless numbers (*Nu*, *Re* and *Sh*) and not the mass flow rate. In fact, it has been shown that further research is required in order to properly combine these models without reaching into paradox results (section 5.2).

## 6.2. Proposals for future work

For the estimation of the precipitation factor ($k_1$ in Singh et al., $k_M$ in IHMT) the radial to convective mass transfer ratio (*Sh*) is calculated based on the wax concentration profile. That profile is entwined with the temperature profile and the relevant equations (51)(52) are solved together. For ease of reference these equations are:

$$Nu = \frac{(-2r_i)\frac{\partial T}{\partial r}\Big|_{r=r_i}}{T_b - T_i} = \frac{2r_i h_i}{k_{cond}^{oil}} \quad (51)$$

*and*

$$Sh = \frac{(-2r_i)\frac{\partial C}{\partial r}\Big|_{r=r_i}}{C_b - C_i} = \frac{2r_i k_M}{D_{wo}}. \quad (52)$$

The mechanistic model provides a well-established heat transfer solution for 1-dimensional problem. The 2-dimensional problem though is not addressed. Essentially, there is a need for the radial temperature distribution in the 2-phase flow. In turn that, would give an accurate result on the radial wax concentration profile for the 2-dimensional problem.

Moreover, the diffusion rate $D_{wo}$ must be given in correlation with the GVF as well as the temperature. The diffusion rate probably changes in the presence of bubbles both due to mass transfer and heat transfer variations compared to 1-phase flow.

Finally, the wax deposition models receive as input the dimensionless numbers Re and Nu. But the Re and Nu numbers for two phase flow do not convey the same mass and heat transfer properties in 2-phase flow as they do in 1-phase flow. That error could be alleviated by multiplying the precipitation factor $k_1$ or $k_M$ with a weight term. For example, for 2-phase flow of GVF = 0.1 the weight factor could be '(1-GVF)×Coefficient'. To determine such a function experimental correlations are required for wax deposition in 2-phase flow.

## Bibliography

**A.Kamari A.Bahadori, A.H.Mohammadi** On the Determination of Crude Oil Salt Content: Application of robust modeling approaches [Journal] // Journal of the Taiwan Institute of Chemical Engineers. - 2015. - pp. 27-35.

**A.Meziou R.Tafreshi M.Chaari M.Franchek R.Borji K.Grigoriadis** Low-Dimensional Modeling of Transient Two-Phase Flow in Pipelines [Article] // Journal of Dynamic Systems, Measurement, and Control. - October 2016. - pp. 101008-01 - 101008-17.

**Bai Q.Bai Y.** Subsea Engineering Handbook [Book].

**Bratland Ove** Multi-phase flow assurance [Article] // The Flow Assurance Site. - 2010.

**C.R.Wilke Pin Chang** Correlation of diffusion coefficients in dilute solutions [Article] // A.I.Ch.E Journal. - June 1955.

**Calsep** PVTsim 20 Method Documentation.

**Carslaw H. S., and J. C. Jaeger** Conduction of Heat in Solids [Article] // Oxford Press, Clarendon, 2nd ed.. - 1959.

**Coutinho João A. P.** Predictive UNIQUAC: A New Model for the Description of Multiphase Solid−Liquid Equilibria in Complex Hydrocarbon Mixtures [Journal] // Industrial & Engineering Chemistry Research. - 1998. - pp. 4870–4875.

**Coutinho P.Jerome D. Jean-Luc J.A.P.** Chapter 10: Modelling phase equilibria in systems with organic solid solutions [Journal] // Computer Aided Chemical Engineering. - American Institute of Chemical Engineering Journal. - pp. 229-249.

**Creek J.L. H.J.Lund J.P.Brill M.Volk** Wax Deposition in Single Phase Flow [Book]. - 1999.

**Cussler E. L., S. E. Hughes, W. J. Ward, and R. Aris** Barrier Membranes [Article] // J. Memb. Sci. - 1988. - pp. 38, 161.

**Deen W.M.** Analysis of Transport Phenomena [Report]. - [s.l.] : Oxford University Press, 1998.

**Flatern Rick Von** Offshore [Online] // http://www.offshore-mag.com. - 3 1, 1997. - http://www.offshore-mag.com/articles/print/volume-57/issue-3/departments/technology-focus/deepwater-challenges-paraffins.html.

**H.P.Ranningsen B.Bjorndal** Wax Precipitation from North Sea Crude Oils. 1.Crystallization and Dissolution Temperatures, and Newtonian and Non-Newtonian Flow Properties [Article] // Energy & Fuels. - September 9, 1991. - pp. 5, 908-913.

**Hatch J. R., J. B. Risatti, and J. D. King,** Geochemistry of Illinois Basin Oils and Hydrocarbon Source Rocks: Chapter 24: Part I. Illinois Basin: Oil and Gas Systems [Article] // M 51: Interior Cratonic Basins:. - 1990. - pp. 403-423.

**Hausen H.** Darstellung des Warmeuberganges in Rohren durch verallgemeinerte Potenzbeziehungen. VDI Z., 4, 91 [Article]. - 1943.

**Hayduk W., and B. S. Minhas** Correlations for Prediction of Molecular Diffusivities in Liquids [Article] // Can. J. Chem. Eng.. - 1982. - pp. 60, 295.

**K.S.Pedersen Per Skovborg H.R.Rernningsen** Wax Precipitation from North Sea Crude Oils. 4. Thermodynamic Modeling [Journal] // Energy & Fuels . - 1991. - pp. 924-932.

**Lee H.Su** COMPUTATIONAL AND RHEOLOGICAL STUDY OF WAX DEPOSITION AND GELATION IN SUBSEA PIPELINES [Book]. - Michigan : The University of Michigan, 2008.

**Leontaritis K.J** The Asphaltene and Wax Deposition Envelopes. Fuel Sci. Technol. Int. 14 (1-2): 13-39. [Online]. - 1996. - http://www.tandfonline.com/doi/abs/10.1080/08843759608947560.

**Lira-Galena C. Firoozabadi A. Prausnitz J.M.** Chapter 10: Modelling phase equilibria in systems with organic solid solutions [Journal] // American Institute of Chemical Engineers. - 1996. - pp. 42,239.

**LTD ASIA PROTECH CO.** ASIA PROTECH CO. LTD [Online] // http://www.asiaprotech.com. - 2012. - http://www.asiaprotech.com/emainset.htm?id=pro04&xcode=01&mcode=02.

**Matzain A Apte M. S. Zhang H. Volk M. Redus C. L. Brill J. P. & Creek J. L.** Multiphase flow wax deposition modeling. [Conference] // Proceedings Engineering Technology Conference on Energy.. - Houston, USA : ETCE 17114, 2001.

**N. Petalas K. Aziz** A Mechanistic Model for Multiphase Flow in Pipelines [Article] // Journal of Canadian Petroleum Technology. - June 2000. - pp. 43-55.

**Oosthuizen P.H. and D. Naylor** An Introduction to Convective Heat Transfer Analysis [Book]. - [s.l.] : McGraw Hill, 1999.

**P. Rygg O. B. Rydahl, A. K. Rønningsen H.** Wax deposition in offshore pipeline systems [Conference] // 1st North American Conference on Multiphase Technology. - Banff, Canada. : [s.n.], 1998.

**P.Singh C.Sarica P.** Study the Effect of Condensate Tie-back on Wax Deposition in an Indonesian Offshore Crude Oil Pipeline [Online] // ResearchGate. - May 2014. - https://www.researchgate.net/publication/267461368_Study_the_Effect_of_Condensate_Tie-back_on_Wax_Deposition_in_an_Indonesian_Offshore_Crude_Oil_Pipeline.

**P.Singh H.S.Fogler, R.Venkatesan** Morphological evolution of thick wax deposits during aging [Article] // AIChE Journal. - [s.l.] : AIChE Journal,, May 2001. - pp. 1059-1074.

**P.Singh R.Venkatesan, H.S.Fogler** Formation and Aging of Incipient Thin Film [Article] // AIChE Journal. - May 2000. - pp. 6-18.

**R.Venkatesan H.S.Fogler** Comments on Analogies for Correlated Heat and Mass Transfer in Turbulent Flow [Article] // American Institute of Chemical Engineers. - July 2004. - pp. 1623-1626.

**Robinson K. M.** An overview of source rocks and oils in Indonesia [Conference] // Proceedings, Indonesian Petroleum Association 16th Annual Convention. - 1987. - pp. 97-112.

**Rosvold K.,** Wax deposition models.. - [s.l.] : Norwegian University of Science and Technology NTNU: Trondheim, Norway., 2008.

**S.Cem V.M.** Tulsa University Paraffin Deposition Projects. - [s.l.] : The University of Tulsa 600 South College Avenue Tulsa, Oklahoma 74104., 2004.

**Seider E. N., and C. E. Tate** Heat Transfer and Pressure Drop of Liquids in Tubes [Article] // Ind. Eng. Chem.. - 1936. - pp. 28, 1429.

**Tao Zhu University of Alaska Fairbanks Jack A. Walker ConocoPhillips Alaska, Inc., J. Liang University of Kansas** Evaluation of Wax Deposition and Its Control During Production of Alaska North Slope Oils. - December 2008.

**Terrell Robert** OilPro [Online] // http://oilpro.com. - 2014. - http://oilpro.com/project/1468/girassol.

**Van Driest E.R.** On Turbulent Flow near A Wall [Article] // Aero. Sci. - 1956. - pp. 23,1007.

**Y.Taitel A. E.Dukler** A Model for Predicting Flow Regime Transitions in Horizontal and Near Horizontal Gas-Liquid Flow [Article] // AIChE. - January 1976. - pp. 47-55.

**Z.Huang H.S.Lee M.Senra H.S. Fogler** A Fundamental Model of Wax Deposition in Subsea Oil Pipelines [Book]. - 2011.

## Appendix

## Physical Parameter Interactions